RIGA TECHNICAL UNIVERSITY

Artūrs Brēķis

MAGNETOHYDRODYNAMIC GENERATOR DRIVEN BY A THERMOACOUSTIC ENGINE

Summary of the Doctoral Thesis

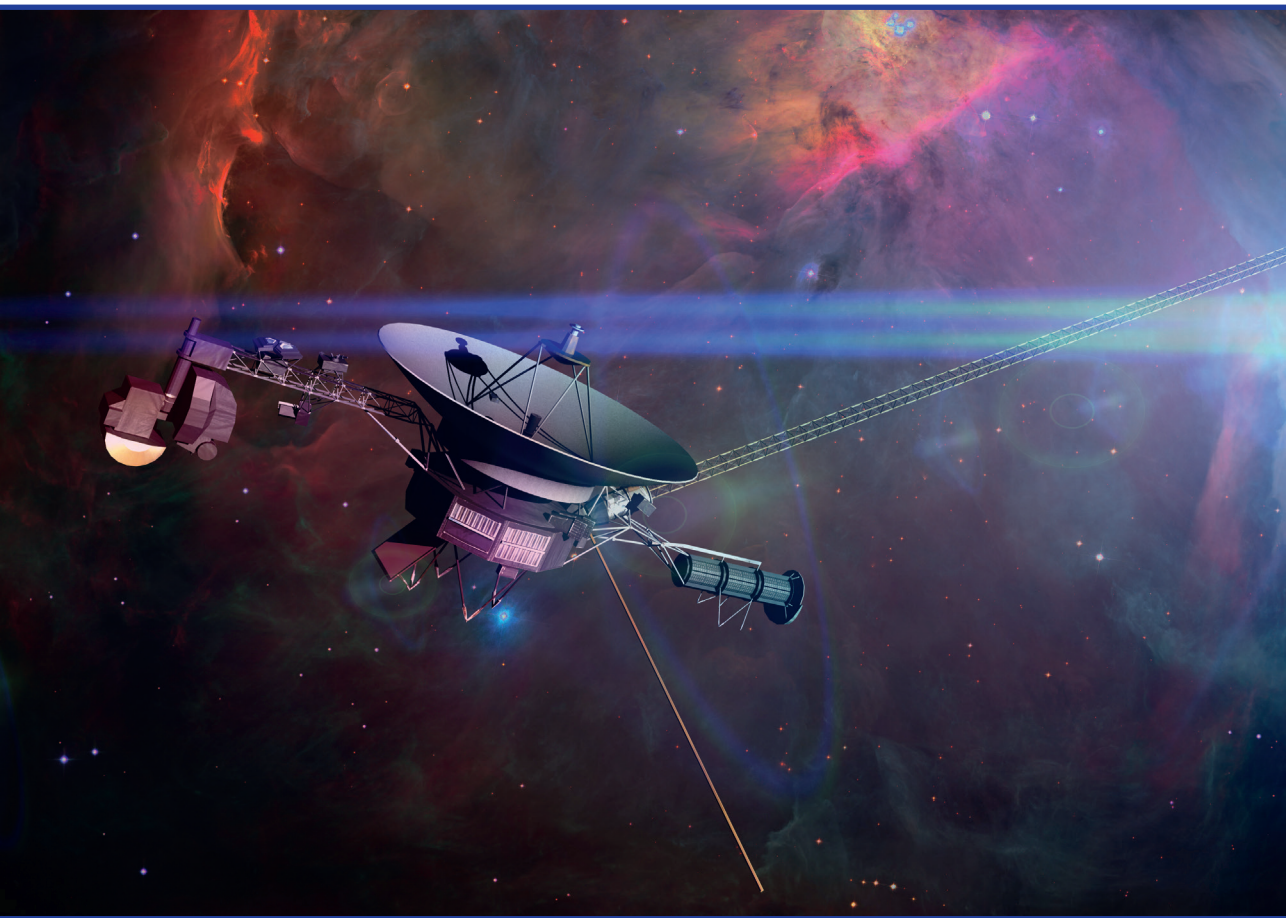

RTU Press
Riga 2023

RIGA TECHNICAL UNIVERSITY
Faculty of Electrical and Environmental Engineering
Institute of Industrial Electronics and Electrical Engineering

Artūrs Brēķis
Doctoral Student of the Study Programme "Power and Electrical Engineering"
Subfield "Electrical Machines and Equipment"

MAGNETOHYDRODYNAMIC GENERATOR DRIVEN BY A THERMOACOUSTIC ENGINE

Summary of the Doctoral Thesis

Scientific supervisors:

Academician, Leading Researcher Dr. phys.
AGRIS GAILĪTIS

Professor Dr. sc. ing.
ANDREJS PODGORNOVS

RTU Press
Riga 2023

Brēķis, A. Magnetohydrodynamic Generator Driven by a Thermoacoustic Engine. Summary of the Doctoral Thesis. Riga: RTU Press, 2023. –53 p.

Published in accordance with the decision of the Promotion Council "P-14" of 20 September 2022, Minutes No. 04030-9.12.2/9.

This research was carried out in the Institute of Physics of the University of Latvia and funded by the "Seventh Framework package FP-7" European project "SpaceTRIPS: Space Thermoacoustic RadioIsotopic Power System", grant No. 312639. It was also partly supported by the RTU European Regional Development Fund project No. 1.1.1.3/18/A/001 "RTU Student Innovation grants," activity "Product development project."

https://doi.org/10.7250/9789934228926
ISBN 978-9934-22-892-6 (pdf)

DOCTORAL THESIS PROPOSED TO RIGA TECHNICAL UNIVERSITY FOR THE PROMOTION TO THE SCIENTIFIC DEGREE OF DOCTOR OF SCIENCE

To be granted the scientific degree of Doctor of Science (Ph. D.), the present Doctoral Thesis has been submitted for the defence at the open meeting of RTU Promotion Council on 19 April 2023 10.00 at the Faculty of Electrical and Environmental Engineering of Riga Technical University, Āzenes Street 12/1, Room 212.

OFFICIAL REVIEWERS

Professor Emeritus Dr. habil. sc. ing. Jānis Dirba,
Riga Technical University

Professor Dr. phys. Andris Jakovičs,
University of Latvia, Latvia

Professor Dr. phys. Valdis Bojarevičs,
Greenwich University, United Kingdom

DECLARATION OF ACADEMIC INTEGRITY

I hereby declare that the Doctoral Thesis submitted for the review to Riga Technical University for the promotion to the scientific degree of Doctor of Science (Ph. D.) is my own. I confirm that this Doctoral Thesis had not been submitted to any other university for the promotion to a scientific degree.

Artūrs Brēķis ……. (signature)
Date: ……

The Doctoral Thesis has been written in Latvian. It consists of an Introduction, 4 chapters, Conclusions, 98 figures, 4 tables, 2 appendices; the total number of pages is 143, including appendices. The Bibliography contains 97 titles.

TABLE OF CONTENTS

INTRODUCTION

The topicality of the Thesis

Electric machines with liquid metal as a working body, or magnetohydrodynamic (MHD) machines, have experienced a great wave of development in recent decades. Today, the demand for magnetohydrodynamic machines such as electromagnetic pumps and MHD generators is growing. Demand has also extended to industries that traditionally used other types of technology, such as aerospace.

On the other hand, the nuclear energy sector is also showing interest in electromagnetic pumps. This type of pumps is increasingly considered as the most advantageous solution in the development of cooling systems for the 4th generation fast neutron breeder reactors.

The main advantage of MHD electric machines is the absence of electrical and mechanical contacts, as well as bearings. Therefore, such a complete non-contact performance opens up the possibility of using them in places where the work safety requirements are the highest. The possibility of using these advantages of MHD machines in long or distant deep space missions is also relevant.

The two directions listed are the main types of MHD electric machines. The present Doctoral Thesis is focused on one of them. The dissertation is devoted to the research of a new generation MHD generator working on a new operating principle. The novelty is further enhanced by the fact that this generator is coupled with a relatively little-known technology called a thermoacoustic engine.

Research object, goals, and tasks

An alternating current magnetohydrodynamic generator powered by a thermoacoustic drive was chosen as the object of research in the Doctoral Thesis.

Purpose of work: **Research and construction of energy converter based on a new type of alternating current MHD generator coupled with a thermoacoustic engine.**

To achieve the goal, the following work tasks are set, which also correspond to the work structure.

Tasks of the theoretical part

1. Application of the existing DC conduction type MHD machine theory to the AC regime using the T-shaped equivalent electric circuit of an electrical transformer.
2. Development of an analytical mathematical model of the MHD generator using electromagnetic field equations combined with hydrodynamic equations.

Tasks of the experimental part.

1. Terrestrial prototype construction and testing in Earth laboratory conditions of the thermoacoustic engine coupled with alternating current MHD generator intended for long space missions.
2. A detailed description of the manufactured facility, as well as an analysis of some of its most important parts and assemblies.
3. Individual tests of the MHD generator alone, separated from the TAc engine, with the aim of studying the electric machine in detail.
4. Separate individual experiments with the TAc engine without the MHD generator.
5. Development of experimental stands for the study of techniques aimed at preventing the generator's liquid metal free surface instability and conducting experiments on them.

Scientific novelty

1. Using the principle of the equivalent circuit of the transformer, a calculation method has been developed for determining the parameters of a new type of AC MHD generator, which is able to observe the real magnetic saturation of the electric machine.
2. The aspects of calculation methods of the DC conduction type MHD generators have been applied and adapted to AC mode, using the transformer circuit approach and the possibilities of numerical calculations of electromagnetic fields with the finite element method (FEM).
3. A calculation method for the MHD generator has been developed using a magnetohydrodynamic equation system written in integral form; a comparison of the two developed methods was made.
4. Proposed solution for the electromagnetic stabilization of the studied MHD generator liquid metal free surface.

Practical significance

1. An automated calculation program in the "Visual Basic for Applications" environment has been developed for calculating the parameters of the MHD generator, which also takes into account the armature reaction.
2. The developed methods can be used in the design and optimization of future AC MHD generators of this type.

Theses to be defended

1. A thermoacoustic engine-driven alternating current magnetohydrodynamic generator with a liquid sodium working body can generate electrical energy.
2. The developed mathematical calculation methods of the MHD generator parameters can be used to evaluate the operating modes of the electric machine under study.

Research tools and methods

Numerical calculations of the MHD generator magnetic field were made with the finite element method software Quickfield. The automation of the calculation with feedback has been performed with the ActiveField technology, using the Visual Basic for Applications (VBA) programming language, in the Excel Macros environment.

Also, for the mathematical representation of the induced electric current distribution in the liquid metal, the Quickfield environment using the electric field mode is used. The calculation of sodium current and electric potential distribution performed with the complex variable approach was conducted in the Matlab environment.

The measurement results of the SpaceTRIPS facility experiments were processed in the Origin PRO software.

Frequently used notations and abbreviations

MHD – magnetohydrodynamics

TAc – thermoacoustics

IPUL – Institute of Physics of the University of Latvia

SpaceTRIPS – abbreviation of “Space Thermoacoustic Radio-Isotopic Power System”

Author's personal contribution

The author was responsible for the development of the thermoacoustic engine and MHD generator prototype. He coordinated its construction and assembly, personally participated in the assembly of the facility, and closely cooperated with the designers from France during the production, constantly consulting in connection with the construction of the equipment so that the prototype was developed according to the designer's drawings. Therefore, the author does not claim the production drawings of the SpaceTRIPS device developed by the French design office SERAS as his own. However, during the development of the device, the author was forced to introduce his own innovations, new parts, and nodes, as well as changes in the original design several times. To illustrate that, the creation of the topology of the real thermoacoustic contour can be indicated. Figure 1.1 shows the device designed in the drawings with compactly bent sound pipes, as well as the stylized T-shaped geometry of the facility actually made by the author. This was done to simplify and facilitate the production and organization of the measuring system.

The author was entirely responsible for the planning, preparation, execution, data processing, and interpretation of all experiments and experimentally acquired data. Calculations using the developed methods and analysis of the results were also under the author’s control. The float experiments, as well as the compressor and loudspeaker benches for liquid metal surface stabilization experiments, were completely authored concept and design.

The work done by the author described in the Thesis is only one part of the large-scale, international scientific project called SpaceTRIPS. As in any technological project, prototyping

is usually an iterative process, with each successive iteration improving on the previous one. Therefore, already at an early stage of the work, the aim was not to immediately produce a perfectly working machine that would meet the best working conditions described in Section 1.1. During the research, the author has identified the shortcomings of the equipment, which should be eliminated when designing similar structures. The project and the Thesis are, therefore, intended to make it possible to realize a competitive electrical machine in the future, which at the present stage (at the time of completion of the Thesis) is far from being the case. Therefore, the realistic plan the author followed during the development of the Thesis was to investigate and test the operation of the first prototype of the device in a small-scale experimental study. Also, to learn about the machine and its design features and to understand what improvements might be made in future experiments or when building the next prototype.

Approbation in conferences

The results of the Doctoral Thesis were presented at the following scientific conferences:

1. **Brēķis, A.** "Magnetohydrodynamic generator driven by a thermoacoustic engine", *11th International Doctoral School of Energy Conversion and Saving Technologies*, Riga Technical University, "Ronīši", Klapkalnciems, May 27–28, 2022.

2. **Brēķis, A.** "Thermoacoustic-to-magnetohydrodynamic energy converter for deep space flights and possibilities to improve it", *18th International Conference of Young Scientists on Energy and Natural Sciences Issues (CYSENI)*, Lithuanian Energy Institute, Kaunas, Lithuania, May 24–27, 2022.

3. **Brēķis, A.** Alemany, A., Freibergs, J. "Analysis of Magnetohydrodynamic Generator Driven by Thermoacoustic Engine for Deep Space Applications", *2020 IEEE 61st International Scientific Conference on Power and Electrical Engineering of Riga Technical University (RTUCON)*, Riga Technical University, Riga, November 5–7, 2020.

4. **Brēķis, A.**, Freibergs, J., Alemany, A., Maurice, M. X., Roy, E., Zeminiani, E., Eckert, S. "Experimental Investigation of Sound Parameters in SpaceTRIPS Facility of Thermoacoustic-to-MHD Energy Converter", *11th PAMIR International Conference of Fundamental and Applied MHD*, University of Reims Champagne-Ardenne, Reims, France, July 1–5, 2019.

5. **Brēķis, A.**, Freibergs, J., Gailītis, A., Alemany, A. "Maiņstrāvas MHD ģeneratora parametru novērtējums", *77th International Scientific Conference of the University of Latvia*, Institute of Physics of the University of Latvia (IPUL), Riga, February 22, 2019.

6. Alemany, A., Francois, M. X., Jeantet P., Poli, G., Zeminiani, E., Eckert, S., Freibergs, J., **Brēķis, A.** "SpaceTRIPS", *The 3rd Russian Conference on Magnetohydrodynamics-2018*, Institute of Continuous Media Mechanics, Perm, Russia, June 18–21, 2018.

7. **Brēķis, A.**, Freibergs, J., Gailītis, A., Alemany, A. "SpaceTRIPS: TAc+MHD iekārtas 2017. gadā paveiktais", *76th International Scientific Conference of the University of Latvia*, Institute of Physics of the University of Latvia, Salaspils, February 9, 2018.

8. **Brēķis, A.**, Freibergs, J., Gailītis, A., Alemany. A. "New Experimental Results from Testing "Space Trips" Facility of Thermoacoustic System Coupled with Magnetohydrodynamic

Generator", *VIII International Scientific Colloquium of Modelling for Materials Processing*, University of Latvia, Riga, September 21–22, 2017.

9. **Brēķis, A.**, Freibergs, J., Gailītis, A. "Termoakustiskā MHD ģeneratora jaunāko eksperimentu rezultāti", *75th International Scientific Conference of the University of Latvia*, Institute of Physics of the University of Latvia, Riga, Latvia, February 3, 2017.

10. **Brēķis, A.**, Gailītis, A. Freibergs, J. "Testing of MHD Generator Prototype for Space Applications", *17th MHD days 2016 conference*, Max Planck Institute for Solar System Research, Göttingen, Germany, November 30 – December 2, 2016.

11. **Brēķis, A.**, Gailītis, A. Freibergs, J. "Thermoacoustic MHD Generator Prototyping and Experiments", *10th PAMIR International Conference of Fundamental and Applied MHD*, University of Cagliari, Cagliari, Italy, June 20–26, 2016.

12. **Brēķis, A.**, Gailītis, A. Freibergs, J. "Termoakustiskā MHD ģeneratora prototipa izstrāde un testēšana", *74th International Scientific Conference of the University of Latvia*, University of Latvia, Riga, Latvia, February 1, 2016.

13. **Brēķis, A.**, Gailītis, A. Freibergs, J. "Termoakustiskā MHD ģeneratora prototipa izstrāde un testēšana", *RTU 57th Student Scientific and Technical conference*, Riga Technical University, Riga, April 14, 2016.

14. Freibergs, J., **Brēķis, A.** "Space TRIPS facility – prototyping and experiments", *AIDAA 2015 Conference on Aeronautics and Astronautics / Aerospace & defense meetings Torino*, Politechnico di Torino, Torino, Italy, November 17–19, 2015.

Publications

The main results of the Doctoral Thesis were published in 8 scientific publications, 5 of which are indexed in SCOPUS and Web of Science:

1. **Brēķis, A.,** Alemany, A., Alemany, O., Montisci, O. Space Thermoacoustic Radioisotopic Power System, SpaceTRIPS: The Magnetohydrodynamic Generator. *Sustainability*, 2021, Vol. 13, No. 23. *Open access*, Available: doi: 10.3390/su132313498, *https://www.mdpi.com/2071-1050/13/23/13498/htm*, SCOPUS

2. Gailītis, A., **Brēķis, A.** Equivalent Circuit Approach for Acoustic MHD Generator. *Magnetohydrodynamics*, 2020, Vol. 56, No. 1, pp. 3–13. ISSN 0024-998X. e-ISSN 1574-0579. Available: doi:10.22364/mhd.56.1.1, SCOPUS

3. **Brēķis, A.**, Alemany, A., Freibergs, J. Initial Experimental Tests on Space TRIPS Facility of Thermoacoustic-to-MHD Energy Converter. *Magnetohydrodynamics*, 2020, Vol. 56, No. 2/3, pp. 255–267. ISSN 0024-998X. e-ISSN 1574-0579. Available: doi:10.22364/mhd.56.2-3.17, SCOPUS

4. **Brēķis, A.**, Alemany, A., Freibergs, J. Analysis of Magnetohydrodynamic Generator Driven by Thermoacoustic Engine for Deep Space Applications. In: *2020 IEEE 61st Annual International Scientific Conference on Power and Electrical Engineering of Riga Technical University (RTUCON 2020): Proceedings*, Latvia, Riga, November 5–7, 2020. IEEE, pp. 1–7. ISBN 9781728195100. Available: doi:10.1109/RTUCON51174.2020.9316584, SCOPUS

5. **Brēķis, A.**, Freibergs, J., Alemany, A. Space Thermo Acoustic Radio-Isotopic Power System: Space TRIPS. *Magnetohydrodynamics*, 2019, Vol. 55, No. 1, pp. 5–14. ISSN 0024-998X. e-ISSN 1574-0579. Available: doi:10.22364/mhd.55.1-2.1, SCOPUS

6. **Brēķis, A.**, Freibergs, J., Alemany, A., Francois, M., Roy, E., Zeminiani, E., Eckert, S. Experimental Investigation of Sound Parameters in SpaceTRIPS Facility of Thermoacoustic-to-MHD Energy Converter. From: *11th PAMIR International Conference on Fundamental and Applied MHD: Proceedings*, France, Reims, July 1–5, 2019. University of Reims Champagne-Ardenne, pp. 191–195.

7. **Brēķis, A.**, Freibergs, J., Gailītis, A., Alemany, A. New Experimental Results from Testing "Space Trips" Facility of Thermoacoustic System Coupled with Magnetohydrodynamic Generator. In: *Proceedings of the VIII International Scientific Colloquium "Modelling for Materials Processing"*, Latvia, Riga, September 21–22, 2017. University of Latvia, pp. 107–112. ISBN 9934182602. Available: doi:10.22364/mmp2017.16

8. **Brēķis, A.**, Freibergs, J., Gailītis, A., Alemany, A., Roy, E., Jeantet, P., Poli, G., Zeminiani, E., Maurice, F., Gerbeth, G., Eckert, S. Thermoacoustic MHD Generator Prototyping and Experiments. In: *10th PAMIR International Conference Fundamental and Applied MHD: Proceedings*, Italy, Cagliari, June 20–24, 2016. University of Cagliari, pp. 606–610. ISBN 978-88-90551-93-2.

ALTERNATIVE SOLUTIONS EXISTING IN THE WORLD

Space technologies: satellites, probes, space stations, etc. that fly near the Sun are usually powered by solar panels [1]. Thus, by using photovoltaic energy converters. However, moving away from the Sun, the radiation intensity per unit area decreases squarely [2]. Therefore, at a very large distance from the Sun, such as in the orbit of Jupiter, to maintain the same developed electric power of the photovoltaic converter as in the typical satellite near the Earth, its area must be enormous [3].

As a solution to this problem, it is possible to use nuclear fuel from radioactive isotopes as the primary energy source [4]. Materials such as plutonium and americium – ^{238}Pu and ^{241}Am – have half-lives of several tens or even hundreds of years, which allow them to release energy for a long time [5]. Nuclear reactions release energy in the form of heat, which can be further converted into electricity. For this purpose, thermoelectric generators can be used, which convert heat into electrical voltage using the Peltier effect. Such technology is advantageous at low powers and has been done on deep space missions such as Voyager, Pioneer, and others [6]. However, thermoelectric converters usually have a low efficiency, which often does not exceed a few percent.

The current vector of evolution for deep Space missions is also focused on the study of Stirling-type or external combustion engines and their modifications [7]–[9]. They have higher efficiency. However, at the same time, the space industry requires high operational reliability for this type of equipment, and Stirling engines with their moving parts cannot fulfill this.

The possibilities of using thermoacoustic (TAc) technologies in space are promising. Thermoacoustic converters are relatively little-known energy conversion devices, the principle of operation of which is based on the mutual interaction of thermodynamic and acoustic phenomena [10], [11]. They are similar to the Stirling-type converters in terms of their operating principle in the thermodynamic sense [12]–[16]. However, they do not have any moving, solid parts and are able to perform mechanical work using gas pressure fluctuations generated during machine operation. Until now, thermoacoustic devices were used in Space technologies only in 1992, in the Discovery shuttle unit. But then, the device served only to cool electronic systems [17]–[19].

As for the electrical power generation stage, it is worth considering the creation of an electric generator with a liquid metal working body, thereby eliminating any solid, mechanically degrading moving parts [20]–[23]. Many different solutions are known for magnetohydrodynamic power plants, where a heated plasma would be flowing through a permanent magnetic field, thus generating a DC voltage [24]–[26]. This technology, however, turns out to be technologically difficult to implement due to the high plasma temperature required and the lack of appropriate heat-resistant materials.

All of the above makes it impossible for the time being to apply the discussed concepts in real deep space missions. Therefore, there is a justified interest in looking for other mechanisms of energy transformation, which have not resulted in significant success so far.

1. TAc ENGINE COUPLED WITH MHD GENERATOR

1.1. Working principle and general overview

The combined system of the thermoacoustic engine and the MHD generator constructed and studied by the author is free from the listed drawbacks, so this type of technology will be especially useful in future flights, for example, in the orbit of Jupiter and beyond. Since the USA is the leading player in the organization of extremely distant missions today, with the development of this project, European science, with the support of the European Space Agency (ESA), strives for technological independence in these types of missions. A step-by-step energy conversion chain characterizing the operating principle of the constructed facility is shown in Fig. 1.1, where it can be seen that the primary energy source is a radioactive isotope, the heat produced by which is directed to a specific sound generator. The sound it produces is, in turn, sent to a specifically designed magnetohydrodynamic generator, producing electricity.

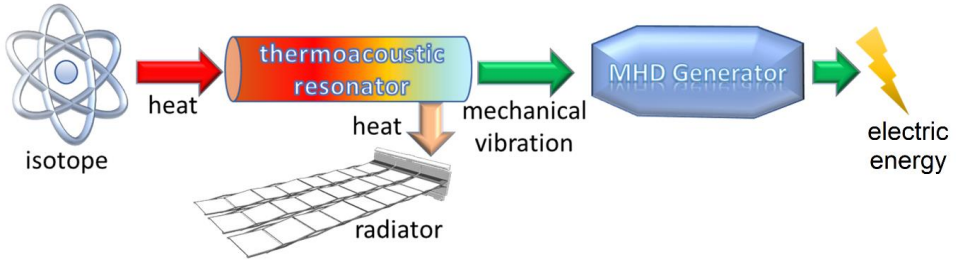

Fig. 1.1. The operating principle of the constructed equipment.

The experimental part of the Doctoral Thesis was carried out with the financial support from the European Commission's 7th Framework Program grant in the project of the Institute of Physics of University of Latvia called Space TRIPS. The consortium of researchers involved in the project forms an international group of scientists in which Latvia had the most important role, since the manufacturing and testing of the prototype was carried out at the Institute of Physics of the University of Latvia in Salaspils. Seven organizations from 5 countries are involved in the project:

- France – CNRS, AREVA, HEKYOM
- Italy – Thales Alenia Space
- Germany – Helmholz Zentrum Dresden Rossendorf
- Netherlands – ASTER Thermoacoustics
- Latvia – Institute of Physics of the University of Latvia (IPUL)

Project coordinator: Professor Dr. phys. Antoine Alemany, “HEKYOM”, France, Grenoble.

The technology has gained interest of the US private company Deep Space Industries as well as of the European Space Agency, to whose representatives the author has repeatedly presented the results of research.

Before starting the description of the equipment, the author would like to note once again that the **technological drawings and 3D models** shown in the following section are not created by the author and are included in the work only for illustration purposes, in agreement with the project coordinator and project participants.

The thermoacoustic engine transforms thermal energy into mechanical energy – a standing sound wave, thus generating pressure oscillations [27]. This mechanical energy is converted into electrical energy by the MHD generator using an electromagnetic induction [28], [29]. This is achieved by moving a liquid, electrically conductive metal, specifically sodium [Na], at about 100 °C, in a magnetic field due to pressure oscillations, periodically reversing the direction of the liquid's motion. The choice of molten Na as the working body of an electric machine is justified by the fact that from all metals, it has the highest electrical conductivity in the liquid state: $\sigma_{Na} = 10.36 \cdot 10^6 \frac{S}{m}$. The high conductivity makes it possible to observe the strongest magnetohydrodynamic interaction while other conditions, for example, magnetic field, remain unchanged. At the same time, the density of sodium at its melting point of 97.8 °C is low: $\rho_{Na} = 928 \frac{kg}{m^3}$ [30]. This, in turn, makes it possible to obtain the most favorable conditions for the machine's operation in terms of fluid inertia. This is essential in this case due to the fundamental principle of operation of the proposed technology, which is already based on the acquisition and use of pressure oscillations to create an oscillating fluid flow in the electric machine [31]. Advantages of the device:

- Fully contactless performance, without any mechanically degradable, moving solid parts or bearings.
- High expected overall efficiency: under the best conditions up to $\eta_{MHD+TAC} \approx 25$ %, compiled by the MHD generator efficiency $\eta_{MHD} = 70$ % and efficiency of TAc engine $\eta_{TAc} = 35$ %.
- Quasi-static mode of operation, especially suitable for space. Quasi-static here means that the kinetic energy of the TAc engine is transferred to the MHD part only due to the gas movement.
- Ability to directly obtain 50 Hz sinusoidal AC voltage.

In Fig. 1.2, a 3D model of the technology is presented, both coupled and by separating the two machines individually. The technology is designed and the drawings are developed in Grenoble, France, in the engineering office of the SERAS-CNRS laboratory. On the other hand, the prototype was manufactured at the IPUL sodium laboratory of Magnetic Hydromechanics. During the production of the prototype, the design and its individual components were optimized and improved by the author according to the needs, but the operating principle and concept were kept unchanged.

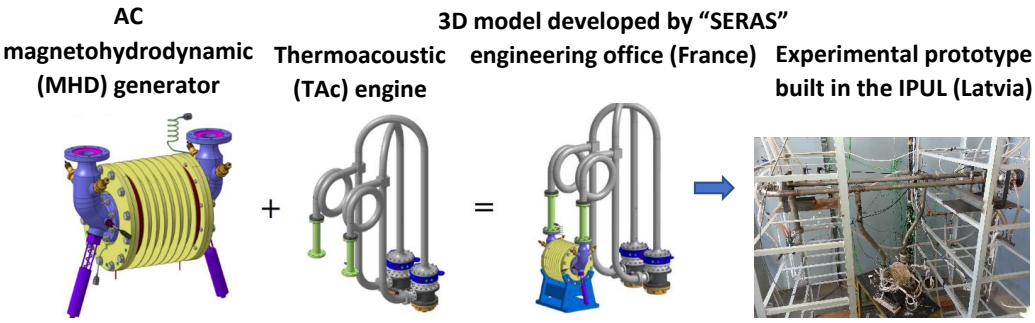

Fig. 1.2. The designed model of the combined system of a thermoacoustic engine and MHD generator (a, b, c), as well as a photo of the actual prototype (d).

1.2. Thermoacoustic engine

The thermoacoustic effect is a thermodynamic process that allows the conversion of thermal energy into sound energy using the temperature, density, and pressure changes of the selected working gas, as well as their mutual interaction [32]. In the given system, the primary engine is considered to be a thermoacoustic engine that acts as a sound generator. Its scheme and components are shown in Fig. 1.3.

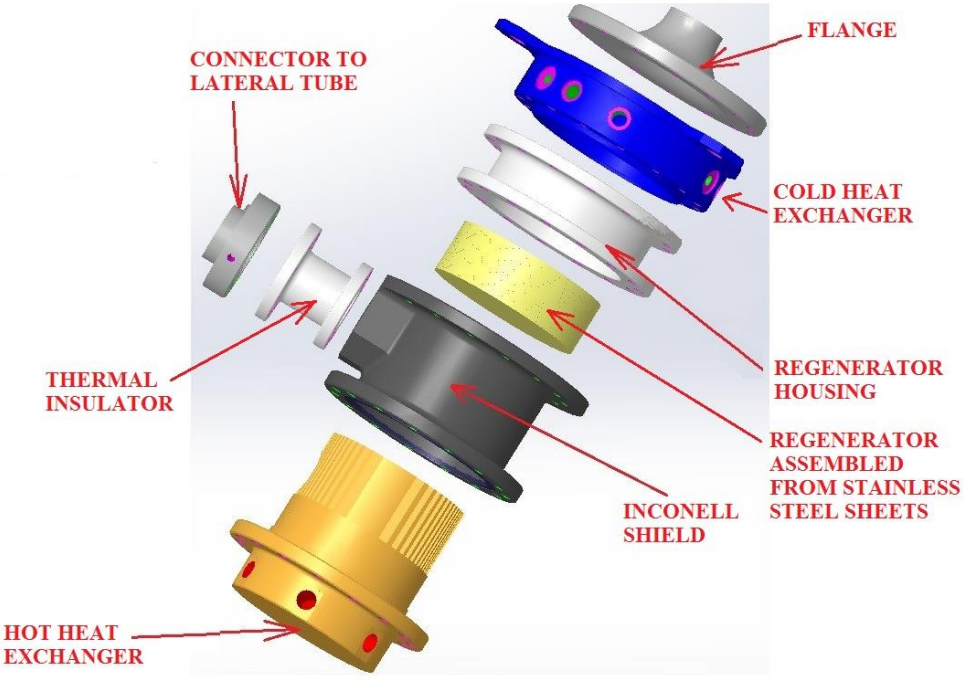

Fig. 1.3. Scheme of the thermoacoustic engine and its components.

The main component of the thermoacoustic engine is a specific heat exchanger with a large heat transfer surface area. In the thermoacoustic literature [33], depending on the engine's modification, it is called a regenerator or a stack. The regenerator is isolated from the surrounding environment with a zirconium oxide ring insulator. It is placed between two heat exchangers, the cold one and the hot one – heated to a high temperature of 800 °C. A temperature of around 20 °C is maintained in the cold heat exchanger. The hot heat exchanger made of Inconel steel brand is heated by electric heaters in the form of special coils wound with nichrome and kantal wires, where the coils, in this case, simulate radioactive heaters. This heat exchanger is covered with a casing or shield made of the same brand of Inconel material, to which a sound circuit is added through an additional ceramic heat insulator.

The low temperature, on the other hand, is obtained using a cold heat exchanger. It is a complex part with a specific labyrinth inside it through which, under laboratory conditions, room temperature water flows, which washes 1,700 small tubes with a diameter of 1.7 mm, through which the cooling gas flows – here, argon.

In a real space application, the scientists of the Italian space technology developer Thales Alenia Space have planned to ensure the cooling of the cold heat exchanger in the form of heat radiation, thus ensuring a cold end temperature of 150 °C, i.e. ensuring that this temperature is also above the melting point of Na, as described in [34] and [35]. On the other hand, the engineers of the French nuclear energy company AREVA have planned to use radioactive Americium modules as heating elements of the hot heat exchanger in the potential future space prototype. These modules could be at the same temperature as in the laboratory experiment – the already mentioned 800 °C.

In general, the design of a TAc engine can be created both in a tube of finite length, creating a standing sound wave, and in a closed loop, creating a traveling wave. The given facility implements the second case but in series with another TAc engine of the same type, which creates a toroidal loop in which both connected TAc engines act as amplifiers of the resulting excited traveling wave [36]. On the other hand, in the so-called TAc transformer tubes, the induced traveling wave is transformed into the standing wave. The nominal data of the TAc facility are shown in Table 1.1. Each of both TAc engines is rated at 500 W.

Table 1.1

Nominal Parameters of the TAc Engine

Working gas	Mean pressure	Pressure oscillation amplitude	Total introduced thermal input power for TAc facility	Acoustic output power	Expected Carnot efficiency	Hot heat exchanger temperature	Cold heat exchanger temperature
Argon	40 bar	+/– 6 bar	1000 W	350 W	66 %	800 °C	20 °C

The amplitude, frequency, and other parameters of the sound wave depend on [12]:

- environment for sound wave propagation – geometries of pipes, as well as heat exchangers and regenerator;
- type of inert working gas and its physical properties where the wave propagates;
- temperature gradient in the regenerator, or, in short, temperature difference at its ends;
- mean pressure of the working gas used (pressure above normal atmospheric pressure).

At a certain supplied gas mean pressure, in the conditions when the temperature difference at the ends of the regenerator exceeds a critical value, a pressure wave is spontaneously generated, which propagates in the tube at the speed of sound. This results in the generation of sinusoidal oscillations around mean pressure. This also explains the excitation of a said traveling wave. In the Thesis, such a critical excitation curve has been experimentally acquired.

This observation is consistent with the fact that sound is, by definition, gas pressure oscillations propagating through the medium as an acoustic wave. In this mode, acoustic energy flows from one TAc engine to another in the pipe circuit. Part of the power, in turn, goes to the outputs where the MHD generator is connected. In the T-shaped branches of the mentioned outlets (in Fig. 1.4, acoustic transformer tube connection points for the sound circuit), gas sound velocity has a maximum value, but pressure oscillations are minimal. On the other hand, when measuring the pressure at the location of the MHD generator itself, the picture is the opposite – the oscillations have a maximum, but the speed is close to zero. The given observation should be explained by the phenomenon of resonance in the engine – the coincidence of the imposed oscillations in phase with the free oscillations. However, in this case, there are only free oscillations – there is no external source of oscillation, as one TAc engine boosts and amplifies the other. Resonance mode can be obtained by appropriately adjusting the geometry of the machine – pipe lengths, cross-section, etc. [37]. Here, a contradiction could arise with the definition of free oscillations, namely that they must always be decaying. However, in this case, the oscillations are continuously maintained artificially by the two TAc engines.

A single TAc engine design is also possible, but this option has several drawbacks, such as the need for an external acoustic starter, and is more sensitive to even small geometric changes in the acoustic topology, in other words, regarding the MHD generator [10], [11], [33].

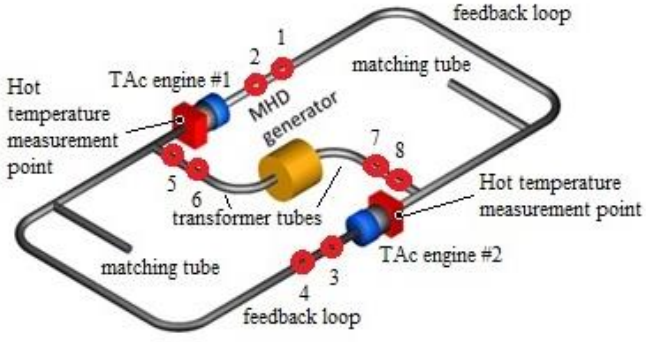

Fig. 1.4. Scheme of the SpaceTRIPS loop.

1.3. Alternating current magnetohydrodynamic generator

The sound coming from the TAc engine causes molten sodium in the annular channel of the MHD generator to oscillate in the axial direction. Radially magnetized samarium-cobalt (Sm_2Co_{17}, with coercive force Hc = 817 kA/m) permanent magnets directed to the central axis of the electric machine create a permanent magnetic field in the active part – the annular sodium channel – which induces a closed azimuthal alternating current in the moving liquid metal. The pulsating magnetic field produced by this AC current sums by the principle of superposition with the magnetic field produced by the permanent magnets and induces a time-varying electromotive force in the coil of the electric machine. Therefore, when a load is connected to the winding, a sinusoidal AC current begins to flow through it. It means that the necessary condition for the current generation is the motion of the electrically conducting, liquid medium with respect to the magnetic field, since it is clear that a stationary magnet by itself will not induce anything in the winding. The electrical machine has a coil with 400 turns and uses standard enameled single-strand copper wire with a 0.6 mm diameter.

So, the sodium current generation process includes three orthogonal vectors:

1) Na oscillating flow velocity in the axial direction: **v**(t);
2) the applied magnetic field in the radial direction created by the permanent magnets: **B**(z);
3) electric field in azimuthal direction: **v**(t) x **B**(z).

The last one was measured in an empty Na channel and had a value of 0.33 T.

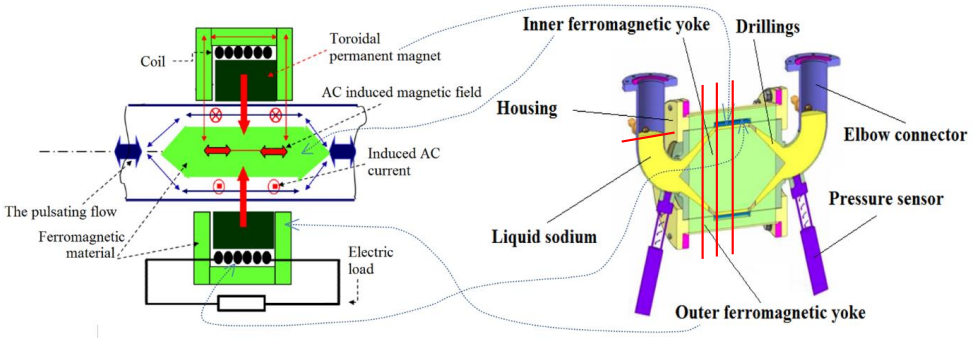

Fig. 1.5. Axial section of the MHD generator model with explanations.

Table 1.2

Characteristic and Nominal Parameters of the MHD Generator

Na temperature	The amplitude of Na movement	Oscillation frequency	Expected output power	Na mass	Outer diameter
100–120 °C	±25 mm	50 Hz	200 W	480 g	200 mm

The outer part of the electric machine's magnetic circuit is made of traditional, radially laminated electrical steel, grade M400-50A, while the inner part is made of high-quality ferromagnetic material – Somaloy. Produced by the Swedish company Höganäs, this magnetically soft material is a dielectric made of epoxy resin compressed and fused with fine iron filings coated with a nano-coating. The material used ensures very low magnetic losses from eddy currents. It has also been experimentally proven in the IPUL that it does not react with sodium. This is essential because the given structural element is in direct contact with liquid metal during electric machine operation.

The design is axially symmetrical in the active part of the electrical machine, and the axial section of the 3D model developed by the CNRS designers is shown in Fig. 1.5. It should be noted here that the magnet system of the generator is not made of a single annular, monolithic, radially magnetized permanent magnet. It is made of 16 identical, sectioned, mutually electrically isolated, sector-shaped magnets arranged in a circle, which are closely adjacent to each other in the form of a ring. Apart from the technological advantages due to the more convenient and simpler fabrication, it is also important from an electromagnetic point of view, thus tending to reduce the azimuthal eddy currents induced in the permanent magnet material due to the resulting changing magnetic field. The reason for these currents is the relatively high specific electrical conductivity of the magnet material. The liquid metal is contained in the volume formed by a total of 0.2 mm thin, welded, Grade2 titanium shell. It separates the sodium from the permanent magnet. The values shown in Tables 1.1 and 1.2 are the input data selected and accepted by the designers as nominal parameters of the generator [34]. Knowing, for example, the displacement and frequency of Na, it is possible to express the velocity of fluid movement and vice versa. The ends of the Na channel are closed by flanges made of titanium, manufactured using 3D printing technology for metal products.

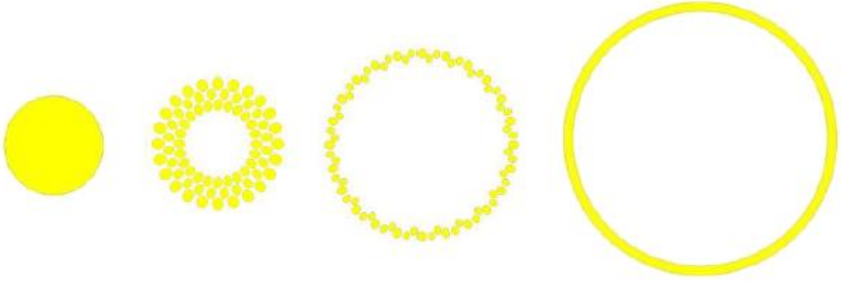

Fig. 1.6. Dynamic change of the Na flow channel through several electric machine cross-sections, corresponding to Fig. 1.5.

As can be seen, the generator requires a transition from an annular fluid channel to a cylindrical one with a constant total cross-sectional area. In order to obtain such a transition, 72 azimuthal multi azimuth boreholes of different diameters of a specific configuration were drilled in the Somaloy core that was glued from separate disks. Figure 1.6 shows a successive transition from an annular channel in the magnetic field zone to a circular cross-section in the elbow connector that forms the free surface of liquid metal. The given figure shows how the

cross-section dynamically changes according to Fig. 1.5 to the right, with the highlighted red lines moving from right to left.

The Na ring channel is partially closed by ceramic insulators at both ends, shown in Fig. 2.2 in red. They are incorporated to at least partially eliminate the undesirable end effects characteristic to MHD machines, which results as induced, parasitic, shunting eddy currents at the ends of the channel [38]–[41]. Such parasitic currents are generated because the magnetic field is no longer constant. At the magnet ends, it drops significantly to almost zero. End-effects in the electrical machine and MHD literature are traditionally known as phenomena associated with the finite lengths of inductors, coils, MHD pumps, and other electromagnetic devices. This often leads to electromagnetic field inhomogeneities at the ends of the equipment and elsewhere.

Also, in the case of the studied MHD generator, the mentioned shunting currents adversely affect the operation of the electric machine. It negatively affects the operation of the electric machine. These currents are represented in the transformer circuit as active resistance R_0. The mentioned aspect is discussed in more detail in Chapter 2 on the theoretical study of the electric machine.

Looking at the parameters of the MHD generator shown in Table 1.2, it can be seen that the magnetic Reynolds number is small due to the small dimensions of the device. It should be noted here, however, that such a classical approach would only consider local processes associated with a single fluid flow in a channel. However, starting to wonder what the Rm value might be for the whole generator, and remembering that the electromagnetic energy conversion process is also very much due to the ferromagnetic parts of the MHD generator, the Rm value may be in the order of unity. In this case, it indicates that the induced magnetic field is having a sensible impact on the applied magnetic field. It also matters how the characteristic size is chosen within the Rm number.

When performing numerical modeling of the magnetic field, visually, the effect of this induced field is clearly visible. This can be seen by comparing the models of the initial applied and resulting field, shown in Fig. 2.7, which is presented in Chapter 2. A quantitative assessment of the armature reaction is shown in Fig. 2.6, where it can be seen that the induced magnetic field plays a noticeable and measurable role in the studied electrical machine energy diagram. In this figure, comparing, for example, the maximum efficiency for the case without a secondary field and that with a nominal load of 200 W, it can be seen that the secondary magnetic field reduces the efficiency of the machine by 2 %. Such a reduction, as can be seen, is relatively small. However, when comparing the cases at higher load resistances, the drop is already higher, and with a significant increase in load, the reduction already starts to play a significant role. Considering the above, the resulting deformation of the magnetic field to a greater or lesser extent also occurs at an Rm number less than 1.

2. EQUIVALENT ELECTRICAL CIRCUIT FOR MHD GENERATOR ANALYSIS

2.1. Formulation of transformer equivalent circuit approach

The AC MHD generator under study can be considered as consisting of two electrical machines:

1. Conduction-type AC MHD generator for converting liquid Na hydrodynamic flow energy into electric energy, represented in Fig. 2.1 with a blue dashed line.
2. A transformer that converts the induced sodium current into an electrical voltage suitable for the consumer (the rest of Fig. 2.1).

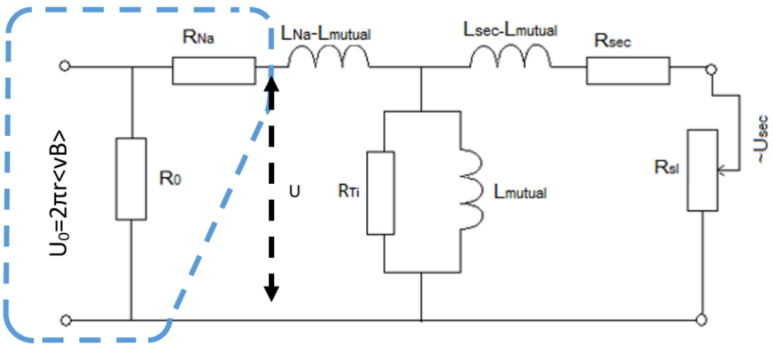

Fig. 2.1. Proposed equivalent electrical circuit of the MHD generator.

Conduction-type MHD pumps and flowmeters are liquid metal devices in which MHD interaction occurs due to an applied magnetic field and a current externally applied to the liquid metal in a conductive manner [28]. This means using power leads that come into direct electrical contact with a liquid metal or channel, which is usually also made of electrically conductive material. In contrast, in induction-type MHD machines, currents in the liquid metal are excited due to electromagnetic induction [40], [41]. Although the theory of conduction-type MHD machines is used in the Thesis, the electric machine under actual study is an inductive-type energy converter, since the current is not supplied in a conductive way.

Taking this into account, it is possible to analyze the operation of the MHD generator using the equivalent T-shape electrical transformer circuit. In addition, the diagram shows the shunting active resistance R_0 characterizing the electromagnetic end effects that are typical to MHD machines. On the other hand, due to the characteristics of Somaloy, the magnetic losses are small and are not taken into account in the diagram.

In the proposed MHD generator calculation method, it is assumed that the local velocity of Na throughout the channel volume is constant. The developed MHD generator calculation method includes an electric machine analysis consisting of 2 steps. First, the knowledge of the geometry of the MHD generator and its magnetic field is converted into the equivalent transformer circuit widely used in the theory of conventional electric machines (Fig. 2.1).

Secondy, further calculation of the equivalent circuit currents and voltages, from left to right (or vice versa), leads to all the necessary parameters of the electric machine.

As already mentioned, in order to analyze the operation of the generator, it is necessary to know the distribution of the magnetic field in the working gap of Na. For the purpose of demonstrations, automated mathematical models of magnetic fields created in the Quickfield environment have been used in combination with a program developed in the VBA programming language to calculate the parameters of the equivalent circuit.

While operating in magnetostatic, axysimmetric mode, three different distributions of the machine's magnetic field were solved using the Finite Element Method (GEM):

1. Only the model of the main magnetic flux field created by the permanent magnets, which serves as a reference field in the further calculation.
2. The magnetic field induced by the currents flowing in the liquid metal.
3. The magnetic field induced by the current flowing in the generator coil.

In addition, two separate electric current distributions in liquid metal, in the plane-parallel mode, were addressed:

1. The main current, induced in liquid Na.
2. Na response current, which is the accumulation of charges on the surface of ceramic insulators.

The response current is mathematically understood as the current induced by the zero current boundary conditions on the surface of the ceramic insulators. The current perpendicular to the surface of the insulator is set to zero, which in turn means that if a certain number of current lines enter a point on the insulator, then the same amount of current must leave the insulator. Of course, physically, no current flows into the insulator, and this must be understood as a mathematical judgment. Therefore, although the principle is similar here, the introduced response current should not be treated as a displacement current, which only plays an important role at high frequencies. To summarise: the response current must be understood as a compensating current induced by the appropriate boundary conditions on the insulators, which compensates the term $vB(z)$ with the opposite sign. These issues are discussed in more detail in the section on conformal representations, where an analytical calculation of the potential and Na current distribution is demonstrated.

In the theory of conduction-type MHD energy converters, issues related to insulators of this type have been extensively studied and reflected in the fundamental literature [28], [29]. For example, it is known that the current distribution is significantly different when the magnetic field is confined along the current leads (Fig. 2.2 b)), or if the field is carried significantly far from the electrode area (Fig. 2.2 a)). The impact also depends on how fast the magnetic field falls at the ends of the studied area (the so-called "end effects" already discussed). As can be seen in Figure 2.2 b), the induced current vortex results in currents flowing against the base current in the area outside the magnetic field. Thus, the regions of the conductive medium before and after entering the magnetic field zone serve as parallel or shunting branches of the electric scheme in the equivalent transformer circuit. Consequently, this results in the efficiency

decrease of the electrical machine. At the same time, there is a way to improve it by inserting an insulating partition of electrically non-conductive material at the entrance and exit of the magnetic field. Thus, in Fig. 2.2 b), the eddy current vortex can be split into two smaller ones. Increasing the number of insulators increases this division proportionally even more. This end-effect reduction technique, suitably adapted, has also been applied to the electric machine under study. The 2nd and 3rd magnetic field models were also used to calculate the inductances of the transformer equivalent circuit using Quickfield.

It is assumed, first, that all the vectors under consideration are orthogonal (e.g. v and B in Equation (2.2) are perpendicular to each other). Second, only one, dominant component of the vector is used. In this case, the vector notations are no longer needed and are discarded. Then, for the description of the current-generating part corresponding to the conduction part of the MHD generator, an expression for the induced current density can be used, written in a way that takes into account the corresponding directions of the electric fields [37]:

$$j(x) = \sigma[vB(z) - E_v(x) - E_U(x)]. \tag{2.1}$$

Taking into account what has just been said in connection with vector notations, for example, in Formula (2.1), the magnetic field is actually considered equal to $\boldsymbol{B} = \{B_r(z); 0; 0\}$, which means the dependence of the radial component on the "z" coordinate. The velocity, in that case, would accordingly be written as follows: $\boldsymbol{v} = \{0; 0; v_z = const\}$. Averaging Equation (2.2) over azimuth and radius yields the following one-dimensional expression, where "(z)" represents the dependence of the quantity on the spatial coordinate in the axial direction only:

$$j(z) = \sigma[vB(z) - E_v(z) - E_U(z)]\,. \tag{2.2}$$

This azimuthal current flowing in the liquid metal is the sum of three mathematically independent terms: the magnetic induction term $vB(z)$ (denoted here by *x* as the 3D coordinate $x = r, \varphi, z$) and two electric field terms, $E_U(z)$, determined by the input voltage corresponding to the transformer part and

$$E_v(z) = v \int B(z_1) g(z, z_1) \mathrm{d}z_1 = vb(z)\,, \tag{2.3}$$

which is the response of ceramic insulators to the term $vB(z)$. This counteraction results in the generation of an electric field, and this is explained by the fact that charges accumulate on the surface of the insulator, which does not allow current to flow through this area. $vB(z)$ and $E_v(z)$ members are proportional to the liquid metal flow rate and linearly dependent on the spatial distribution of the magnetic field. $E_U(z)$, in turn, depends on the electric load and occurs as a result of changes in the magnetic flux. $E_U(z)$ is important because it is needed to calculate the input voltage of the transformer equivalent circuit.

The electric field terms (second and third terms) of Equations (2.1) and 2.2) are written with a minus sign because they act opposite the term $vB(z)$. The quantity $b(z)$ is formed using a formal Green's funtion $g(z, z_1)$ in the integral. The purpose of the Green's function here is that it shows the weight with which a magnetic field at a point "z_1" produces an electric field at another point "z", according to Equation (2.2). In the numerical calculation with the Finite Element Method, the entire integral (2.2) can be calculated at once. However the mentioned Green's function can also be obtained separately, using the complex variable function and conformal mapping approach [42].

As known, power is equal to

$$P = Fv, \tag{2.4}$$

where F is force and v is sodium velocity. On the other hand, the elementary electromagnetic force density df in the elementary volume dV, can be written as

$$\mathrm{d}f(x) = j(x) \times B(z)\mathrm{d}V. \tag{2.5}$$

In that case, the power received by sodium can be expressed as the integral of the ordinary product of $j(x)$ and $B(z)$ without considering $j(x)B(z)$ as a vector scalar product in the following expression:

$$P_{Na} = v \iiint j(x)B(z)\,\mathrm{d}V =$$

$$= \iiint (\sigma v^2 B(z)^2 - \sigma v B(z)E_v(x) - \sigma v B(z)E_U(x))\,\mathrm{d}V\,. \tag{2.6}$$

Expression (2.6) can be simplified and transformed by splitting it into two integrals and introducing the already-mentioned auxiliary term $b(z)$. After performing the integration operation in two coordinate directions, the following equation with two simple integrals is obtained:

$$P_{\mathrm{Na}} = \sigma v^2 \iiint (B(z)^2 - B(z)b(x))\,\mathrm{d}V - \sigma v \iiint (B(z)E_U(x))\mathrm{d}V =$$

$$= 2\pi r h \sigma v^2 \int (B(z)^2 - B(z)b(z))\mathrm{d}z - 2\pi r h \sigma v \int E_U(z)\,B(z)\mathrm{d}z \tag{2.7}$$

From the equivalent circuit, the current through the Na resistance can be written as

$$I_{\mathrm{Na}} = \frac{U_0 - U}{R_{\mathrm{Na}}}. \tag{2.8}$$

Here U_0 is transformer input voltage and U is voltage at the circuit point behind the Na active resistance. Then the power expression for the transformer circuit can be written as follows:

$$P_{\mathrm{Na.ekv}} = \frac{U_0^2}{R_0} + (U_0 - U)I_{\mathrm{Na}} + UI_{Na} = U_0^2\left(\frac{1}{R_0} - \frac{1}{R_{\mathrm{Na}}}\right) - \frac{U_0 U}{R_{\mathrm{Na}}}\,. \tag{2.9}$$

In this way, Expressions (2.7) and (2.9) should be equal.

Primary winding or generating side elements of the equivalent circuit – R_{Na}, U_0, R_0 – can be calculated from the following considerations:

1. Sodium electrical resistance:

$$R_{\mathrm{Na}} = \frac{2\pi r}{\sigma h l_{\mathrm{active}}}, \tag{2.10}$$

is the ohmic resistance to the current flowing in the annular, ring type Na channel with volume

$$\Omega = 2\pi r h l_{\mathrm{active}}\,. \tag{2.11}$$

Although the Na channel is closed and the current through this ring closes on itself, the Na ring still has a finite electrical resistance. R_{Na} is calculated as the ratio of the length of the channel to the specific electrical conductivity of Na and the cross-sectional area of the channel, where h is the height of the channel and l is the axial length. However, in the case of an MHD machine, the distribution of electric potential and current density is not uniform across the Na cross-section, so the current lines are curved, as shown in Fig. 2.2. This leads to the fact that the cross-section $l_{\mathrm{active}}h$ actually used by the current exceeds the free area $l_{\mathrm{free}}h$ of the duct and therefore

the resistance decreases slightly. Figure 2.2 is taken from the textbook dedicated to the theory of conduction-type MHD pumps [28]. However, this image is supplemented by the insulators embedded in the MHD generator under study (in red). Research [28] conducted in IPUL under the supervision of J. Birzvalks has proven that for conduction-type MHD machines

$$l_{\text{active}} = l_{\text{free}} + 2 \cdot 0.22d \ ,$$

where $0.22 \approx \frac{\ln 2}{\pi}$.

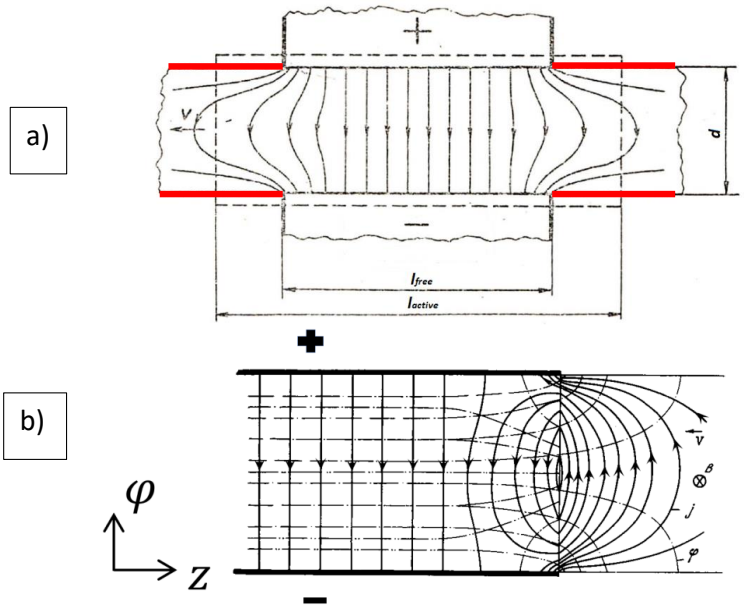

Fig. 2.2. a) – The profile of the current formed by EMF induced in Na, representing the electric current distribution in one subchannel (distance "d") [28]; in red – ceramic insulators corresponding to Fig. 2.4.; the magnetic field is carried far outside the electrode area; b) – induced current profile in the case where the magnetic field is confined to the electrode tips.

To explain the connection of the scheme shown in Fig. 2.2 with the generator under study, one should imagine the Na ring channel as consisting of several subchannels, where one rectangular subchannel is depicted in the mentioned drawing. However, it is worth noting that the actual machine is more complicated than the one shown in Fig. 2.2. The actually created subchannels in the insulators are not rectangular but in the form of circular, axially unsymmetrical (but symmetrical to azimuth) boreholes.

2. To calculate U_0, a numerical electric field model is built, where Quickfield calculates the following dimensionless distribution:

$$N(z) = E_U(z)\frac{2\pi r}{U} \ . \qquad (2.13)$$

By equating the last terms on the right sides of Equations (2.7) and (2.9), the result can be obtained:

$$U_0 = \sigma v R_{\mathrm{Na}} \iiint \left[\left(\frac{E_U(x)}{U}\right) B(z)\right] \mathrm{d}V =$$

$$= \frac{1}{2\pi r} 2\pi r h \sigma v R_{\mathrm{Na}} \int \frac{E_U(z)}{U} B(z) \mathrm{d}z = 2\pi r v \langle B \rangle \ , \qquad (2.14)$$

where $\langle B \rangle$ is the weighted average value of the magnetic field $B(z)$ in the area under consideration, with weight $N(z)$:

$$\langle B \rangle = \frac{1}{l_{active}} \int N(z) B(z) \mathrm{d}z \ , \qquad (2.15)$$

where *N*(z) is weight function. It should be noted that integration here is done over the entire calculation area. In this case, it means to the end of the insulators, where, at the same time, the magnetic field also drops to zero.

3. For the calculation of R_0, the first members of (2.7) and (2.9) are equated, resulting in the following expression:

$$\frac{1}{R_0} = \sigma \left(\frac{\iiint ([B(z) - b(x)] B(z)) \mathrm{d}V}{(2\pi r \langle B \rangle)^2} \right) - \frac{1}{R_{\mathrm{Na}}} \ . \qquad (2.16)$$

Similar to the previous integrals, here also azimuthal integration leads to a 1D formula, where the function depends only on one, namely the axial coordinate z:

$$\frac{1}{R_0} = \left(\frac{\frac{\int ([B(z) - b(z)] B(z)) \mathrm{d}z}{l_{\mathrm{active}} \langle B \rangle^2}}{R_{\mathrm{Na}}} - 1 \right) \ . \qquad (2.17)$$

Based on the proposed MHD generator calculation method, it is possible to obtain the theoretically expected characteristic curves of the electric machine. One of the families of characteristic curves, that is, the obtained efficiency of the MHD generator, depending on frequency and load, is shown in Fig. 2.3.

Such results can be obtained by mathematical modeling of the electric and magnetic fields of the machine, according to the described equations. Figure 2.4. shows the current and

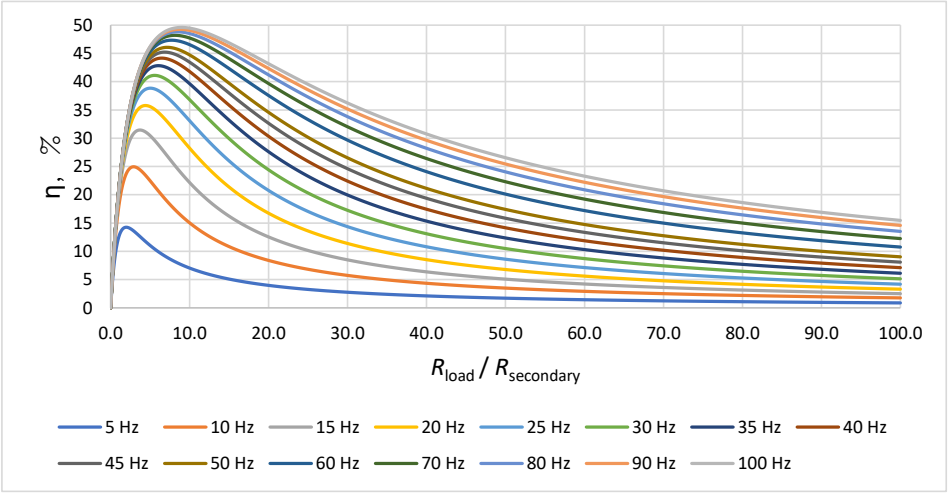

Fig. 2.3. Calculated theoretical efficiency of the MHD generator as a function of load.

potential distributions for the base current and the response current at the ends of one subchannel.

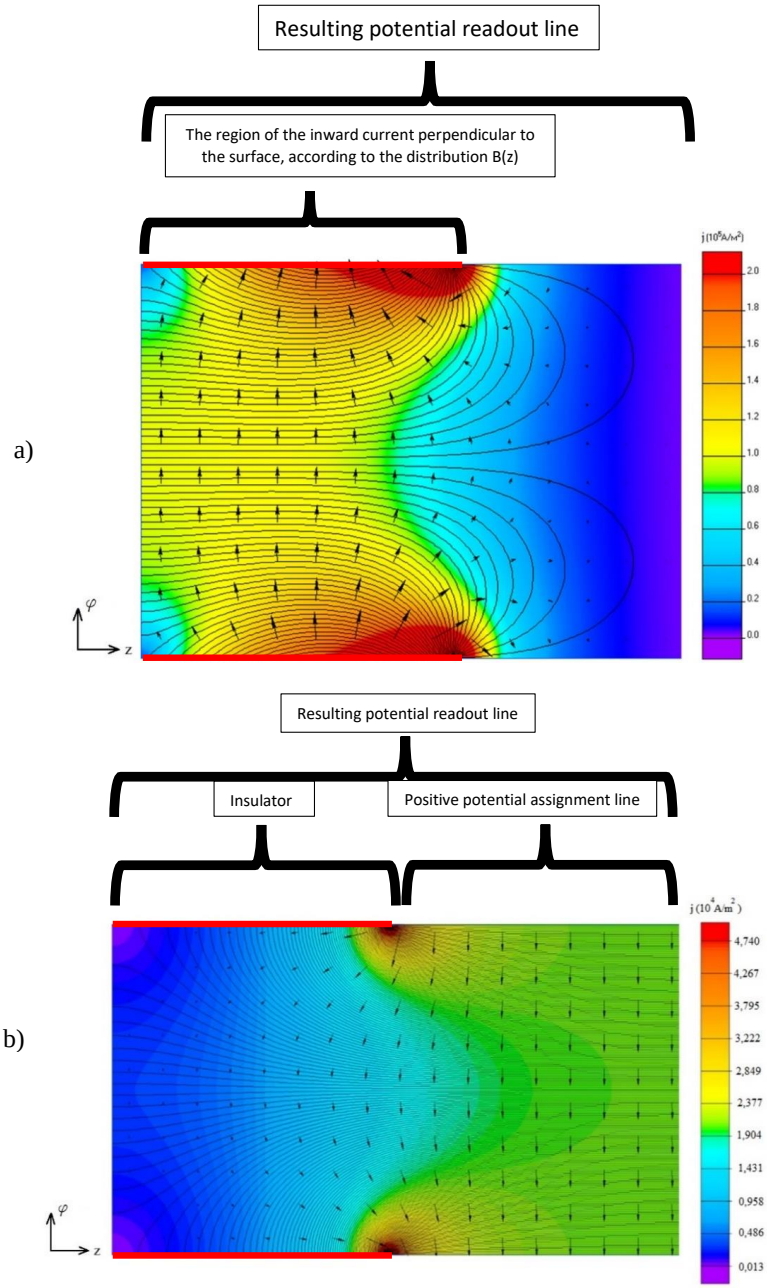

Fig. 2.4. Model of the MHD generator's liquid Na current distribution in one subchannel on its left-hand side: a) – the numerically obtained Quickfield response current; b) – the corresponding base current; places of ceramic insulators are shown in red according to Fig. 2.2 a).

2.2. MHD generator parameter calculation, taking into account the influence of the armature reaction field

The above is valid in the low power mode when the magnetic fields of the currents induced in the liquid metal and the coil modify (reduce) the permanent magnet field a little. At higher power, the field modification can become a limiting factor. This phenomenon is known as the armature reaction in the theory of classical electric machines. In this work, an approach has been developed to take into account the effect of this phenomenon on the operation of the MHD generator.

In magnetohydrodynamics, the magnetic Reynolds number (Rm) is most often used to describe the phenomenon under study, using one of its most primitive interpretations, which states that the ratio of the induced magnetic field to the applied field is proportional to Rm. As already mentioned, the magnetic Reynolds number is small due to the machine's small size. As will be seen, this leads to a small effect of the armature reaction in the nominal 200 W mode. However, as the results obtained in the current paragraph show, the armature reaction still has its stable place in the overall energy balance of the MHD generator.

The novelty of the high-power mode over the low-power one is that the value of the shunt resistance R_0 of the replacement circuit has a time dependence. The calculation is started as in the low-power mode, that is, from the primary field created by the permanent magnets. Next, after setting the required electrical resistance of the consumer, in the Excel environment in VBA (Visual Basic for Applications) language, the developed program code calculates the circuit from the left side (input voltage – U_0) to the right until it stops at the load current and voltage drop on the load resistance. Once all the required currents are found, they are fed into the next Quickfield numerical simulation using Active Field technology [43], [44] (Fig. 2.5), which results in finding the new field distribution. The data from the newly found magnetic field distribution, in turn, already enters the input of the equivalent transformer circuit again, and it continues until the entire AC period is calculated. Therefore, the specific distribution of $R_0(t)$ has been found. Next, integration over the entire AC period gives the dynamics of electric machine's efficiency decrease at different developed power levels.

The principal algorithm of the developed program for the calculation of the influence of the armature reaction is shown in Fig. 2.6. Influence of the calculated armature reaction on the MHD generator's efficiency is shown in Fig. 2.7, at 50 Hz. Comparing the visible curves, it can be observed that as the load increases, the peak of the curve shifts to the side of the lower load resistance. This can be explained by an increase in the proportion of inductive currents in the transformer equivalent circuit, in particular, the middle – magnetization branch current increase. In Fig. 2.8, a comparison is shown of an electric machine's magnetic field unaffected by the armature reaction and also considering the armature reaction.

Fig. 2.5. Used Excel and Quickfield interconnection diagrams.

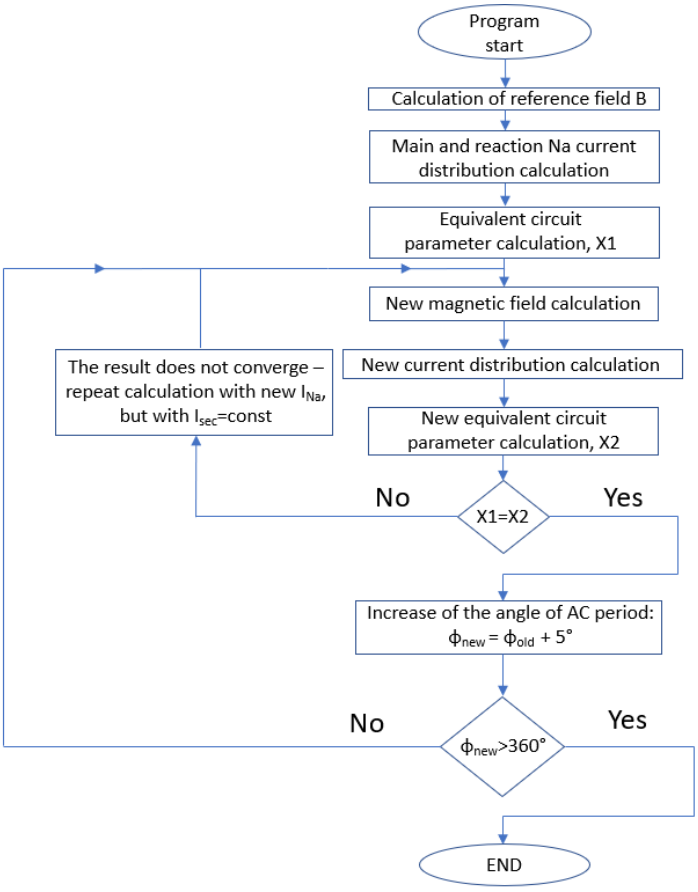

Fig. 2.6. MHD generator armature reaction calculation block diagram.

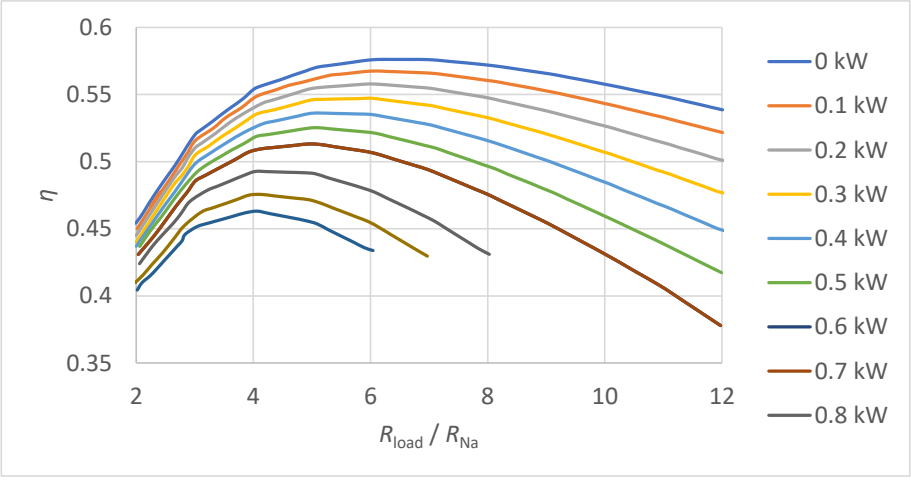

Fig. 2.7. Impact of the resulting calculated secondary magnetic field on the efficiency of the machine during generated useful power mode and without secondary currents.

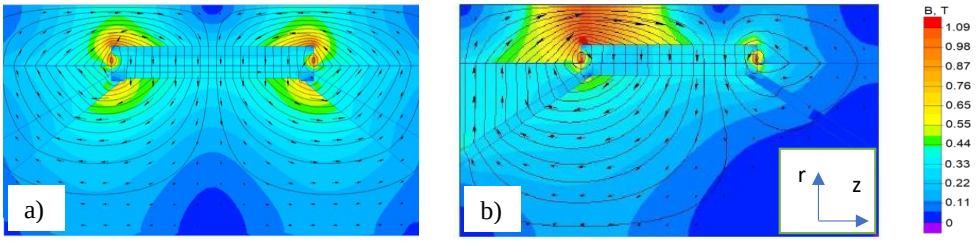

Fig. 2.8. a) – Distribution of the reference field of the MHD generator, or the main magnetic flux induction vector created by the permanent magnets, in a 2D model, in an axial slice;b) – the magnetic field of the MHD generator affected by the armature reaction.

2.3. Complex variable functions for calculation of electric current distribution in liquid metal

It is also possible to analytically calculate the distribution of the electric potential, as well as the current leakage in the liquid metal, using the approach of conformal mapping. This technique means the conformal representation of one complex plane $z = x + iy$ in another complex plane $Z = X + iY$. The point of this representation is that the solution of the Laplace equation, which can be easily found in one geometry, is represented in a different one – in the particular geometric region of interest.

The statement of the task can be formulated as follows. In the general case, the electric potential distribution is described by Poisson's equation:

$$\Delta\varphi = div\,(\boldsymbol{v} \times \boldsymbol{B})\ . \tag{2.18}$$

However, in the configuration under study, neither "B" nor "v" depend on the azimuthal angle. The corresponding vectors are oriented so that $div\,(\boldsymbol{v} \times \boldsymbol{B})$ is zero. This leads to the use of the Laplace equation, already mentioned, instead of the Poisson equation, which has 0 on the right-hand side.

There are several limitations to the proposed approach. First, it applies to the plane-parallel problem. Since the studied electric machine has an axially symmetric geometry in its central, active part, it is necessary to transition from the cylindrical coordinate system to Cartesian coordinates. Such a transition can be made correctly enough, as the condition that the Na-channel mid-radius must be significantly larger than the channel height is fulfilled. Second, to make such a change, it is necessary to cut the annular canal in one place and straighten or bend it. This geometric transformation is performed while keeping the same distribution of electric fields so that instead of an axially symmetric problem, a planar problem is solved. In this context, the following assumptions are made for the calculation:

1. The electric potential is constant over the height of the channel.
2. One of its subchannels is considered instead of a cylindrical Na channel.
3. Only one side of the symmetrical subchannel is considered.

The applied boundary condition derived from the current density expression can be written as

$$vB(z) = E_v(x)\,. \tag{2.19}$$

This means that on the surface of the insulator, in the direction of the normal, i.e. perpendicular to it, incoming currents are zero. It follows from the boundary conditions that the mapping from one plane to the other takes place with the exception of an infinitely long array of straight cuts. These discontinuities also correspond to nonconducting insulators inserted into the Na channel.

The biggest difficulty for such an approach is finding the functional relationships that connect the two complex planes. The following analytical function, valid for representing the response current of Na, was found to be

$$\Phi_{\text{reakc}}(z) = \frac{1}{\pi}\{\ln[\sin(\pi[(x+iy)+a])] - \ln[\sin(\pi[(x+iy)-a])]\}, \qquad (2.20)$$

where a is the distance between 2 adjacent charges in the conformal plane (Fig. 2.9, top), seen between the marginal charge and the vertical edge of green rectangle in Fig. 2.9. Such a potential is generated by an infinitely long array of linear field line sources and leakages, as shown on the top in Fig. 2.9. If the *x*-axis is a field line of any $\Phi_{\text{reakc}}(z)$ potential, then for the potential $\Phi_{\text{reakc}}\big(z(Z)\big)$ all *Z*-plane cuts are part of the same field line, so the corresponding boundary conditions are satisfied.

In this case, the following Green's function is valid for Equation (2.3):

$$g(x, x_1) = \frac{2}{\pi}\ln\left|\frac{\sin\big(\arccos(e^{-\pi x}) + \arccos(e^{-\pi x_1})\big)}{\sin\big(\arccos(e^{-\pi x}) - \arccos(e^{-\pi x_1})\big)}\right| . \qquad (2.21)$$

The drawings obtained during the calculations are shown in Fig. 2.9. In practice, conformal representation means that the plane is "folded" along the line of a specific fold. The upper, horizontal, green fold line in Fig. 2.9 (top) corresponds to the blue centre line in Fig. 2.9 (bottom). This blue line is also the insulator separating the Na subchannels. The folding is done by folding the green line so that the two ends of the line join together, thus representing the half-plane of the upper drawing in the lower image. It should be understood that this figure represents the current distribution before integration using the Green's function. This means that in Fig. 2.9 (bottom), only the outgoing and incoming current lines from a single point are obtained.

From this figure, we can see how the induced term $\boldsymbol{v} \times \boldsymbol{B}(z)$ develops at a given point:

$$x = \frac{-\ln|\cos \pi a|}{\pi} = 0.37381 \quad . \qquad (2.22)$$

For the representation of the base current, the relation of one complex plane to another can be represented by the following function:

$$\Phi_{\text{pam}}(Z) = 1 - \frac{2\arccos e^{-\pi Z}}{\pi} = N(z) \ , \qquad (2.23)$$

where *N*(*z*) is the weight function introduced earlier in the numerical modeling section. Such a division into weight and Green's functions allows us to separate and determine two different weights. One of the two mentioned weights is the one shown in Fig. 2.9 (bottom), where part of the current lines wraps around the insulator. The other weight determines how many current lines flow to the nearest neighboring isolators.

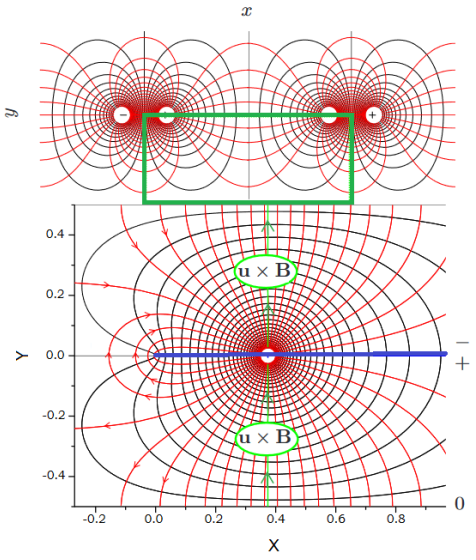

Fig. 2.9. One subchannel model of the Na current distribution: 1) induced response current obtained by the conformal mapping, aimed at the counter direction of the main current (bottom); 2) inverted complex plane (top)

3. MHD GENERATOR ANALYSIS USING VOLTAGE EQUATIONS

3.1. Magnetohydrodynamic equation system

This chapter presents an alternative approach to the use of transformer equivalent circuit. It is based on derivations of analytical equations for currents, Na velocity, and other quantities [45]. These functions are obtained using the MHD equation system in integral form, in one-dimensional approximation, i.e. without numerical modeling. As shown, the developed method gives adequate results that are comparable and agree well with those obtained by the transformer circuit approach, as well as with experimental results [46]. However, before the description of the proposed method, in the author's opinion, it is useful to write in differential form the general system of MHD equations on which the approach is based [47]–[49].

For slowly moving, isotropic and non-magnetic, electrically conductive media, the system of electromagnetic field equations can be written as follows:

$$rot\ \boldsymbol{H} = \boldsymbol{j}, \tag{3.1}$$

$$rot\ \boldsymbol{E} = -\frac{\partial \boldsymbol{B}}{\partial t}, \tag{3.2}$$

$$\boldsymbol{j} = \sigma[\boldsymbol{E} + (\boldsymbol{v} \times \boldsymbol{B})]\ , \tag{3.3}$$

$$div\ \boldsymbol{B} = 0\ , \tag{3.4}$$

$$\boldsymbol{B} = \mu \boldsymbol{H}\ . \tag{3.5}$$

When considering processes in an incompressible, liquid, electrically conductive medium (liquid metal), the equation of fluid flow continuity (3.7) is added to the system of Equations (3.1)–(3.5), as well as the equation of fluid motion, which in hydrodynamics is called the Navier-Stokes Equation (3.6):

$$\rho\left[\frac{\partial \boldsymbol{v}}{\partial t} + (\boldsymbol{v}\ grad)\boldsymbol{v}\right] = -grad\ p + \eta \Delta \boldsymbol{v} + \rho g + [\boldsymbol{j} \times \boldsymbol{B}], \tag{3.6}$$

$$div\ \boldsymbol{v} = 0\ , \tag{3.7}$$

where: t – time;

ρ – liquid metal density;

v – fluid velocity;

p – pressure;

η – fluid dynamic viscosity;

g – gravitational acceleration.

It can be seen that the Navier-Stokes equation includes a term for external forces. In this case, it is the density of the electromagnetic force, and in the MHD processes under consideration, it is often precisely this factor that plays the most important role.

In the proposed MHD generator calculation method, the so-called electrodynamic or solid body approximation is used, which determines that the liquid volume is considered as a moving, solid body. Namely, it is assumed that the local velocity of the fluid is the same at all points in the volume [50].

The model is based on the application of Ampere's theorem. This states that the magnetic field created by the Na current is produced by the induced currents flowing in the sodium (Fig. 3.1.). In the figure, it can be seen that a total of 3 different electric currents pass through the area bounded by the magnetic flux line: Na current I_1, induced current due to losses in the conducting titanium wall I_w, as well as the induced secondary current in the generator coil/load I_2. It can be expressed mathematically by writing Ampere's theorem, in which the integration contour is taken as the magnetic induction vector flux line marked in Fig. 3.1 in red:

$$\frac{B_0}{\mu_0} l_0 + \frac{B_f}{\mu_f} l_f + 2\frac{B_e}{\mu_0} l_e = I_1 + I_2 n + I_w \,. \tag{3.8}$$

Using the principle of magnetic flux continuity:

$$B_f S_f = B_e S_e = B_0 S_0 \,, \tag{3.9}$$

then combining (3.8) and (3.9):

$$B_0 \left(l_0 + \frac{\mu_0 S_0}{\mu_f S_f} l_f + 2\frac{S_0}{S_e} l_e \right) = \mu_0 (I_1 + I_2 n + I_w) \,. \tag{3.10}$$

Let us denote the following quantity by $L_0^{'}$ and call it the equivalent length:

$$L_0^{'} = l_0 + \frac{\mu_0 S_0}{\mu_f S_f} l_f + 2\frac{S_0}{S_e} l_e \,. \tag{3.11}$$

The magnetic flux can then be expressed as

$$\Phi = \frac{S_0}{L_0^{'}} \mu_0 (I_1 + I_2 n + I_w) \,. \tag{3.12}$$

We write the voltage equations for three separate electric circuits: the current in liquid sodium, the current in the coil, and the parasitic current in the constructive element of the electric machine – the shunting titanium wall/shell.

- The current I_1 refers to an annular channel filled with sodium, with mean channel diameter D and electrical resistance r_1. An applied magnetic field crosses an oscillating liquid sodium flow at a velocity V:

  $$I_1 r_1 + \pi D V B = -\frac{\mathrm{d}\Phi}{\mathrm{d}t} \,. \tag{3.13}$$

  Deriving Expression (3.13) gives:

  $$-\frac{d^2\Phi}{dt^2} = \frac{r_1 dI_1}{dt} + \frac{\pi D B dV}{dt} \,. \tag{3.14}$$

- Current I_2 circuit consisting of a generator coil, an electrical load resistor and a power factor correction capacitor. The latter two form impedance: $Z=R\text{-}jX_{\text{Capacit.}}$, which is shown in Fig. 3.1 for the scheme under study. Then the total resistance r_2 and the capacitance C, which allows charge $q = C \cdot U$ to accumulate on the plates:

  $$I_2 r_2 + \frac{q}{C} = -n\frac{\mathrm{d}\Phi}{\mathrm{d}t} \,. \tag{3.15}$$

After appropriate transformations and mathematical manipulations explained further in the main text of the Thesis, these expressions can be combined with the equation of fluid motion in integral form.

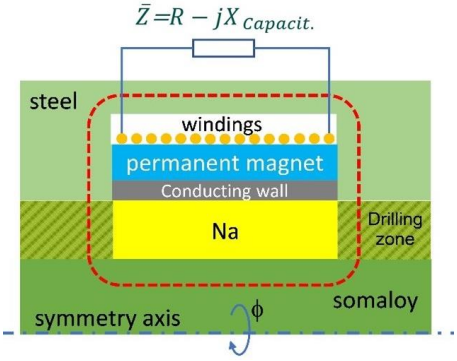

Fig. 3.1. The magnetic circuit under the study of an electric machine.

3.2. Calculation results and their interpretation

Using the proposed approach, the load current, Na velocity, and other expressions are obtained, which can be used for the calculation of the energy and power parameters as well as other characteristic curves of the MHD generator.

For example, in Fig. 3.2 the variation of velocity and load current as a function of load resistance is shown for applied pressure difference $\Delta P = 6$ bar. It can be seen that initially, the resistance starts to increase from zero, at the same time, a rapid increase in Na speed is observed. As the electrical resistance continues to rise above about 200 Ω, the velocity stabilizes and remains constant. On the other hand, it is opposite for the current and, for example, in the case of $\Delta P = 6$ bar starting from the maximum value $I = 5.85$ A, increasing the resistance, the current initially rapidly decreases, after which it asymptotically approaches zero. It indicates that at high load resistances the operation of the electric machine is basically determined by inertial forces.

Figure 3.2 b) shows the calculated electric power and efficiency dependences of impedance at a frequency and mass corresponding to the actually built prototype. As can be seen, the maximum power in this case at ω = 314 rad/s and $m = 0.464$ kg is reached at a resistance of 40 Ω. Looking at the efficiency curve, this peak is shifted in comparison to the power and reaches a resistance of 100 Ω. This means that when choosing the optimal operating mode of the MHD generator, a compromise must be sought between the maximum power and the maximum efficiency of the electric machine. It should be noted that the curves in Fig. 3.2 are obtained only for the MHD generator. This means that the efficiency of the electric machine is separated from the efficiency of the TAc engine.

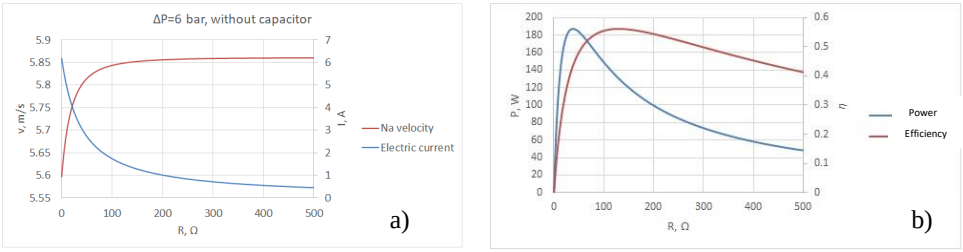

Fig. 3.2. MHD generator Na velocity and load currents (a), as well as electrical power and efficiency (b) dependences on load electrical resistance.

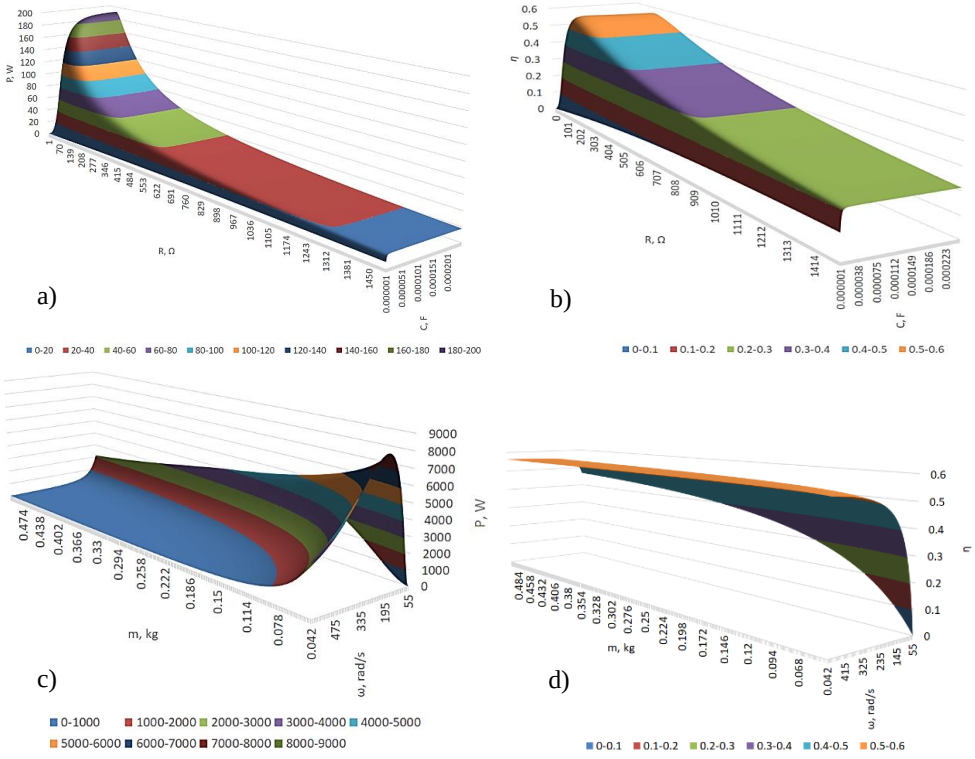

Fig. 3.3. Dependence of the developed useful electrical power (a) and efficiency (b) of the MHD generator on load resistance and capacitor; the same quantities (c) and (d), respectively, depending on the liquid Na mass and the angular frequency of pressure.

It must be remembered that the power factor of an electric machine is always $\cos\varphi < 1$. The phase shift between the load current and voltage affects the maximum possible active power that can be extracted from the MHD generator. By connecting a capacitor of sufficient capacity to the load, it is possible to maximize this power. To reach maximum efficiency, the required capacitance value is, of course, different. This is also observable in Figs. 3.3 a) and b).

Figures 3.3 c) and d) show the dependence of power and efficiency on Na mass and angular frequency, respectively. As can be seen, the power developed decreases with increasing mass because the inertia of the fluid limits the speed of motion at any frequency. On the other hand, as the mass continues to increase, the machine remains increasingly driven by inertial forces, leading to a phase shift angle between Na current and velocity close to $\pi/2$. The consequence of this is that the mechanical power supplied to the generator gets unsatisfactorily low. As can be seen in Fig. 3.3 d), the efficiency tends to a constant value regardless of the sodium mass and at a sufficiently high frequency. These results can be explained by the fact that the model does not take into account the skin effect that affects the Na current at high frequencies.

Questions related to the electromagnetic stability of the generator operation were not investigated in the Doctoral Thesis. However, there is reason to believe that the stable operation of the machine is ensured due to the redistribution of three mutually balanced terms: the applied pressure on the ends of the generator, electromagnetic forces, as well as inertial forces. This means that, for example, if the pressure is suddenly reduced, the current and the Na velocity will automatically settle to a new equilibrium state. This new state depends on the mass of Na, which, in turn, determines the inertia of the system, as mentioned above. This is another reason why possible reduction of Na mass is essential.

Regarding the possible influence of turbulence, it should be noted that the approbation of the method proposed in this chapter has been carried out under laminar flow conditions, and issues related to turbulence have not been discussed. However, some important considerations can be made. First, the transition boundary from laminar to turbulent mode increases with increasing applied magnetic field. Second, the Na flow is not stationary, and the induced secondary magnetic field is also pulsating, as in the given case. Both of these are potential factors in fluid flow instability. Experimentally, individual turbulent structures can be expected to form only at the peak of the oscillation period, when the velocity is maximum. This issue needs to be studied in more detail in the future, but some aspects have been experimentally demonstrated in Chapter 4 of the present Thesis.

The research shows that both proposed calculation methods are adequately comparable, give equally reliable results, and also describe the power, energy, and fundamental parameters of the electric machine in equal detail. When comparing the two calculation methods, inductance and Na velocity are quantities whose use differs between the two approaches. If in the formulation of the transformer circuit the velocity directly appears only at the input of the circuit, then in the method discussed in this chapter, it is operated much more widely.

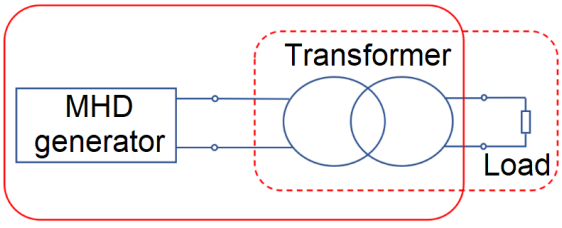

Fig. 3.4. Comparison of the equivalent transformer circuit method and Maxwell's equations approach.

It is also possible to make a comparison in a different way. In Fig. 3.4 the concept of the studied system is shown, with a solid red line separating the calculation approach for Maxwell's equations proposed in this chapter. On the other hand, the dashed red line shows the approach of the equivalent transformer circuit.

4. EXPERIMENTAL STUDIES

4.1. Independent tests of thermoacoustic engine

In order to better understand the operation of the SpaceTRIPS facility and its details when operating in different modes, a large series of experiments were carried out. The constructed thermoacoustic machine and the MHD generator were tested in two ways:

1) by connecting the two devices together as originally intended;
2) by separating the two machines and testing each independently of the other.

Independent tests of the TAc engine were performed by disconnecting the MHD generator and replacing it with an adjustable mechanical valve, thus obtaining the possibility to manually adjust the acoustic resistance of the engine to the sound wave.

In Chapter 1, it could be seen that in Fig. 1.2 c) the geometry of the thermoacoustic engine proposed by the French designers with sound pipes bent in a complex configuration differs from the photo of the manufactured prototype shown in Fig. 1.2. The difference is that in Fig. 4.1 a) the acoustic loop is stretched. The reason for such a change in geometry is the possibility to simplify the construction process, to seal the joints more securely, and to better adapt the loop and measurement system to the laboratory conditions and experimental session. Thus, the actual manufactured device is also created in such a stylized "T" shape. At the same time, the geometry of the acoustic loop has remained the same, thus fully preserving the acoustic performance of the engine without changing its operating mode.

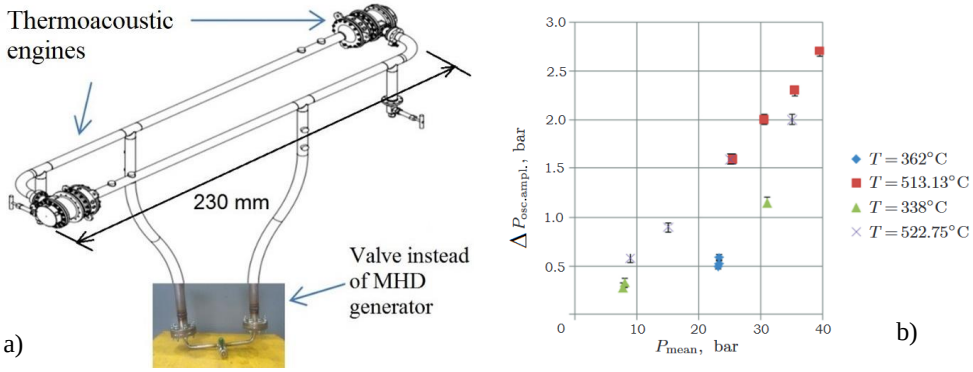

Fig. 4.1. a) – The developed laboratory prototype for individual, separate tests of the TAc engine, replacing the MHD generator with an adjustable, acoustic load in the form of a mechanical valve; b) – the amplitude of pressure oscillations developed by the TAc engine depending on the supplied mean pressure.

Figure 4.1 b) shows the amplitude of the pressure oscillations developed by the TAc engine at different constant temperature differences on the regenerator depending on the mean pressure. It is a summary of experimental results from various tests as the engine develops a stabilized steady state [35]. The tests shown are at the fully closed acoustic load valve position. In this case, the phase shift angle between pressure and sound speed is close to 90° since no useful mechanical power was developed. It can be seen that at a nominal 40 bar mean pressure, the maximum amplitude of pressure fluctuations achieved is 2.7 bar, which was developed at T = 513 °C. This result is satisfactory because the pressure fluctuations typically developed by thermoacoustic engines are usually around 5–10 % of the mean pressure. Such values ensure sufficiently high transmission of sound power to regions with high acoustic impedance, which in this case would be in the liquid metal free surface area of the MHD generator. These issues have been extensively discussed in the thermoacoustic literature [51].

4.2. MHD generator sodium experiments on the developed compressor stand

A special laboratory stand was designed and built for testing the MHD generator independently of the TAc engine (Fig. 4.2). It is based on a suitably rebuilt 2-cylinder 2.2 kW air compressor that simulates the operation of a TAc engine. For this purpose, a compressor has been chosen so that the mutual phase shift of its pistons during movement is 180°. This means that the cylinders work in opposite phases, and when one piston is, for example, in the upper position, the other one is in the lower position. The compressor has been modified by removing its filter and all gas flow one-way valves, leaving the cylinders exposed. Next, a system of manually adjustable valves is connected to the compressor (Fig. 4.2 a), V1–V7), which allows to adjust the output pressure difference. As shown in Fig. 4.2, an MHD generator is connected to this outlet of the valve system. As a result, when the compressor is running, the alternating pressure difference is supplied to the elbows of the generator and, thus, to the free surface of the liquid, causing the Na to oscillate. In Fig. 4.2 a), the red arrows indicate the direction of pressure during the first half-period of the cycle, while the blue dashed arrows indicate the direction in the next half-period. The rotation frequency of the compressor motor was controlled by a frequency converter and was regulated within the range of 15–55 Hz.

The voltage generated in the compressor experiment as a function of time is shown in Fig. 4.3 a). The generator coil and load current plotted on the same time scale is shown in Fig. 4.3 b). The current is represented here in a time domain, which is indicated as the load mode

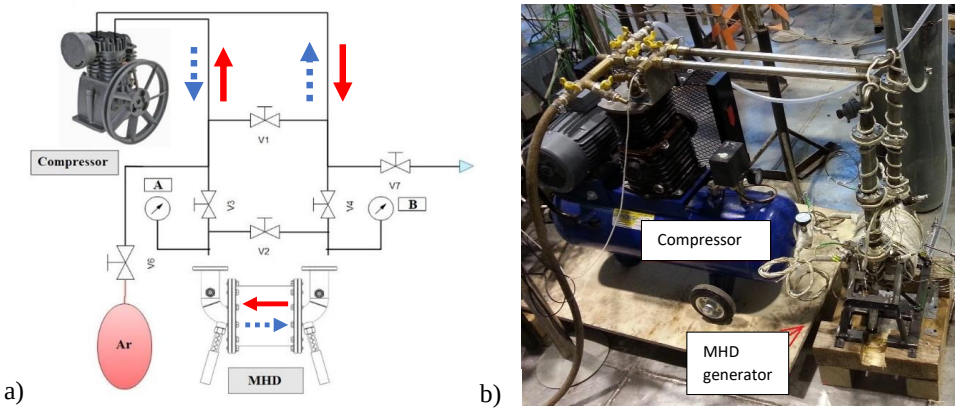

Fig. 4.2. The designed compressor stand for independent tests of the MHD generator: a) – construction scheme; b) – photo of the experimental stand.

in Fig. 4.3 a). An adjustable rheostat is connected to the outputs of the generator coil, which serves as a load.

It can be seen that the largest induced non-load voltage reached an amplitude of 37 V. In load mode, with the highest possible rheostat resistance, 20 V and 0.125 A were obtained, corresponding to 160 Ω. In contrast, 2.5 V and 0.4 A were obtained at the lowest adjusted resistance, giving 6.25 Ω. As shown, the developed voltages and currents are relatively small, which can be explained by the low level of pressure oscillations delivered by the compressor due to its limited power, as well as possible gas leaks through seals, including cylinder rings.

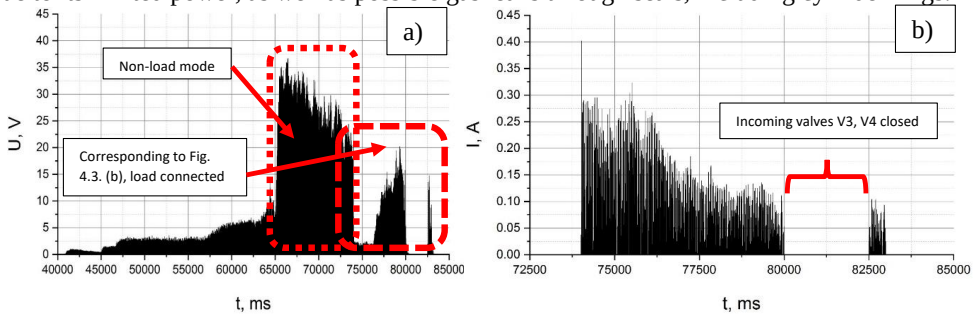

Fig. 4.3. a) – The voltage induced in the coil of an electric machine as a function of time in the compressor + MHD generator experiment with Na; b) – electric current flowing in the MHD generator coil and the load rheostat during the same experiment.

4.3. Model experiments of liquid metal surface stabilizing floats with water

Before Na experiments, the compressor system was tested with water. A bent, transparent, U-shaped tube was used instead of the MHD generator (Fig. 4.4 a)). The justification for such an experiment is the similar physical properties of Na and water, such as density and viscosity, which thus allow modeling the motion of liquid metal. The purpose of the experiment was to visually assess the Na free surface instability and its periodicity, as well as the regularity of the oscillations. The mentioned aspects are essential for the stable generation of electrical output power in a real experiment with liquid metal. As in the Na experiment, in the water test, the volume of the liquid was 0.5 L, and its free surface is shown in Figs. 4.4 b) and c).

The experiment showed that fluid surface oscillations caused by compressor pressure fluctuations are unstable, resulting in irregular, chaotic splashes (Fig. 4.4 a)). The fluctuations of the recorded pressure supplied to the water surface were the same as in the Na experiment of the compressor-MHD generator.

In order to be able to continue the further planned tests, hollow, cylindrical, glass-shaped floats made of 316 L stainless steel have been offered as a temporary solution (Figs. 4.4 b), and c)). They were placed directly on the surface of the liquid (Fig. 4.4 c)). Otherwise, without any artificially created stabilization, it would be reasonable to expect a significant reduction of the induced voltage and, therefore, the generated power at the output of the electric machine. This was also observed experimentally in an independent MHD generator test with sodium without floats.

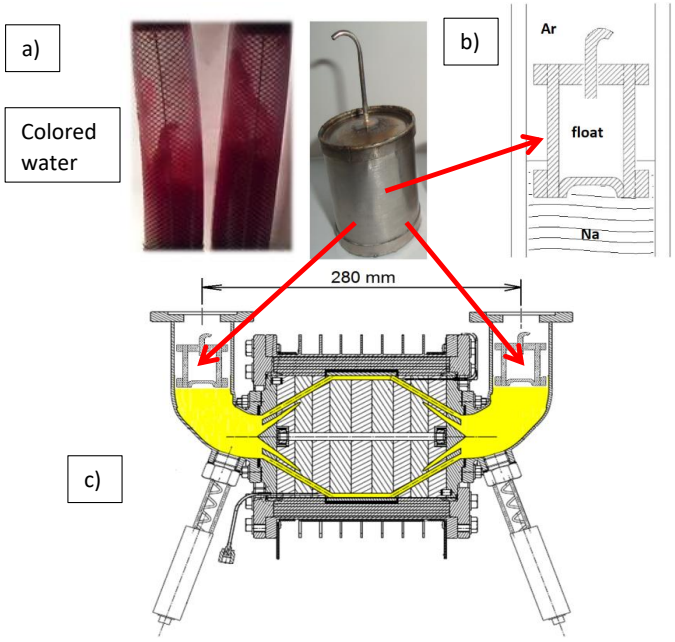

Fig. 4.4. a) – Results of the experiment on the compressor stand with colored water; b) – fabricated Na free surface stabilizing floats; c) – position of the floats in the MHD generator

Several video frames taken in the float water experiment are shown in Fig. 4.5.

A ruler was placed next to the tube to measure the displacement of the float during the full movement. Figure 4.5 a) shows the case where the fluid does not move. On the other hand, Fig. 4.5 b) shows the case when the float has moved away from the equilibrium position as much as possible during oscillation at a frequency of 45 Hz. The same frequency was also adjusted in the Na experiment shown in Figs. 4.2 and 4.3. As can be seen in Fig. 4.5, the maximum displacement of the float is about 2 mm. The surface stabilization effect can be estimated from these frames. They show that the surface of the liquid is still not absolutely flat, as it would be desirable, to allow predictable, controllable and measurable Na mass transfer. However, despite this, the waves observed in a thin layer on the surface of the liquid in the space between the surface of the float and the tube are significantly smaller and less chaotic than in the test with colored water.

a) b)

Fig. 4.5. Experimental video frames from the water test with cylindrical floats.

4.4. MHD generator and thermoacoustic engine coupling experiment

After the independent tests of both machines, the MHD generator was connected to the TAc engine and a coupling experiment was successfully conducted. Output voltage and current oscillogram curves for positive half periods of sinusoids are shown in Figs. 4.6 a) and b) in black, similar to that in Fig. 4.3. In addition to Fig. 4.6 a), on the same time scale, other curves recorded during the experiment are also shown with different colors:

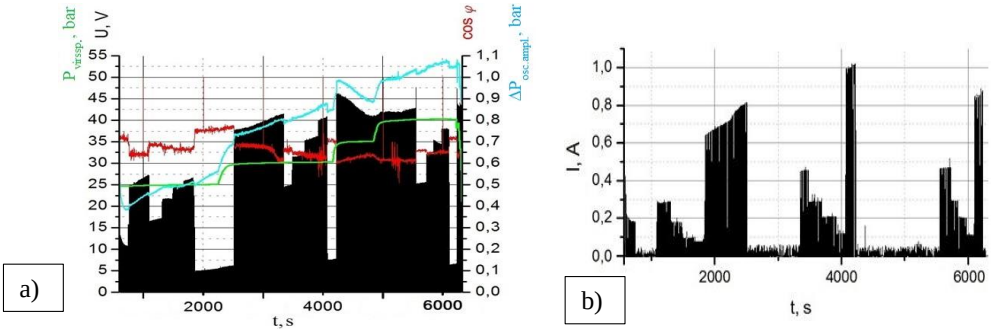

Fig. 4.6. a) – Recorded voltage drop on the load, pressure oscillations, and acoustic power factor in the MHD + TAc experiment; b) – the corresponding recorded load current.

1) green curve – gas mean pressure;

2) red curve – acoustic power factor, or cos φ, where φ is the phase shift angle between the Na flow rate/velocity and pressure curves;
3) blue curve – amplitude of pressure oscillations.

By adjusting the load rheostat resistance, the current and voltage exhibit an exact and expected anti-correlation similar to that observed in the compressor test in Fig. 4.3. As the electrical resistance increases and the current decreases, the voltage increases at the corresponding time. The experimentally developed electric power, as can be concluded from Fig. 4.6, is relatively low compared to the nominal parameters of the generator. However, in this case, the level of supplied pressure oscillations must be taken into account. Comparing

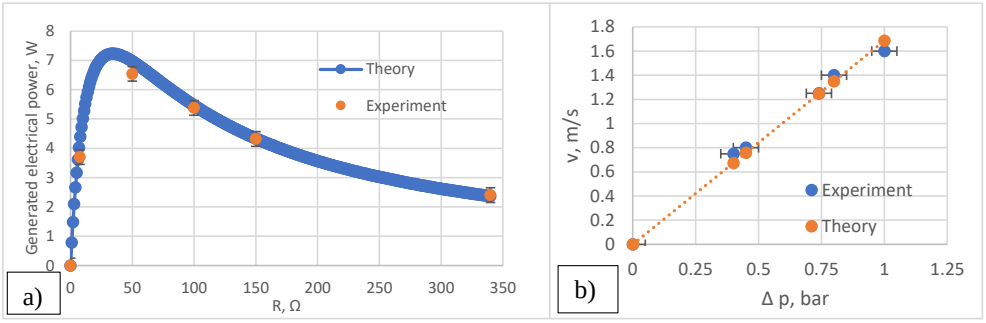

Fig. 4.7. a) – The experimentally developed electric power in the TAc + MHD test and comparison with the theoretical calculation using the method proposed in the Thesis; b) – comparison of the experimentally obtained velocity and pressure with theoretical calculation.

the experimentally obtained data with the theoretically calculated ones at the same developed TAc pressure, a good agreement of the results has been obtained. Such a comparison is demonstrated in Fig. 4.7 a). The given analytically calculated curve is obtained using the developed MHD generator calculation method proposed in Chapter 3 of the present Thesis.

The flow rate was measured using the conduction-type electromagnetic flowmeter, a well-known method in MHD technology. For this purpose, a measuring device with contact electrodes and permanent magnets was specially designed and manufactured [37]. Using the flow measurements and knowing the pipe's cross-sectional area at the specific location of interest, an average value for the Na velocity can be calculated. Figure 4.7 b) shows a comparison of the experimentally obtained Na velocity and pressure $v = f(\Delta p)$ with the one calculated using the MHD equation system approach. It can be seen that the linear relationship obtained here is also in good agreement. The linear nature of the curve can be explained by the fact that pressure and velocity are related to each other by a linear relationship, where the proportionality factor is the complex acoustic impedance. It means that this impedance describes the phase shift between pressure and velocity. This phase shift must be as small as possible for optimal system performance. The theoretical studies carried out in the Thesis have shown that at constant load and frequency, the velocity dependence of the acoustic power factor is linear in the initial part of the curve, namely at low speeds, up to about 5 m/s.

As can be seen in Fig. 4.6, detailed measurements of electric current and voltage were made at three different mean pressures: 25, 30, and 40 bar. The fact that the highest recorded load current of 1 A at 8 V voltage drop on the load resistance can be observed at 30 bar mean pressure and not at 40 may seem unexpected. The explanation for this can be found in the fact that the corresponding temperatures of the hot heat exchangers of the two TAc engines were different and a thermal imbalance of almost 100 °C was observed, which may affect the level of output power produced in the generator. Thermal imbalance means the difference in the readings of the respective two temperature-measuring thermocouples, at the hottest point of each TAc engine, in the hot heat exchanger. The reason for such asymmetry can be found in the fact that the self-made electric heaters implemented in both heat exchangers are not installed precisely the same. This also leads to a low overall TAc + MHD efficiency of 1.6 %.

The total electric power delivered to the TAc engine heaters in this experiment was 250 + 250 = 500 W. The maximum flow rate amplitude in the experiment reached 0.55 L/s, while the oscillation frequency was 58 Hz. It was observed that the experimentally obtained acoustic power factor in some modes is even higher than theoretically predicted.

4.5. A method for electromagnetic stabilization of the liquid metal free surface of an electric machine

As already noted, the main drawback of the developed MHD generator is the existence of a liquid Na free surface, which becomes unstable when the machine operates under certain conditions. Instability, in this case, refers to the oscillations on the flat surface of a fluid, which over time develop into complex, turbulent, chaotic flow structures as instability develops. No technical device should or can have any uncontrollable phenomenon. Therefore, the boundary between argon and sodium must be defined. Otherwise, argon bubbles or gas inclusions can be expected to enter the liquid metal. Failure to address this issue prevents the MHD generator from operating normally.

Further, an original method to solve the surface instability problem for surface stabilization using a non-contact technique is proposed by author. The proposed method is based on the use of an applied, external magnetic field. The lines of the applied field are oriented parallel to the direction vector of the alternating fluid flow, see Fig. 4.8. The transcription of the positions indicated by numbers is as follows:

1) fluid tube;
2) source of the magnetic field;
3) sector in which the magnetic flux lines are parallel to the Na flow streamlines;
4) areas in which the fluid flow crosses the magnetic field lines even in rectilinear motion – in a straight, vertical direction up and down;
5) electrically conductive liquid to be stabilized;
6) the gas above the free surface of the liquid.

In this case, the proposed operating principle can be explained as follows. As soon as one of the liquid layers during the development of instability tries to move away from the rectilinear liquid flow (Fig. 4.8a) – ideal case) trajectory in the space direction – up or down – there will

immediately occur velocity components different from "X" (Fig. 4.8 a)). These velocity components will immediately cross the magnetic flux lines, which in turn will induce electric currents in the liquid metal in the free surface region. The magnetic field, in interaction with the induced currents, will try to set the fluid flow streamlines that have left their trajectory back to their original place. This would result in a stabilizing effect on the surface of the liquid.

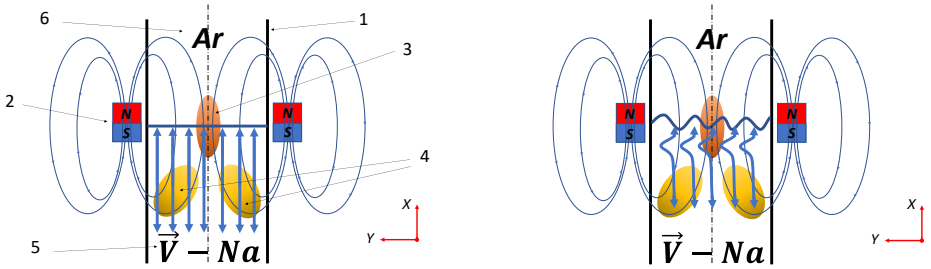

Fig. 4.8. Diagram of the proposed MHD generator liquid metal surface stabilization method.

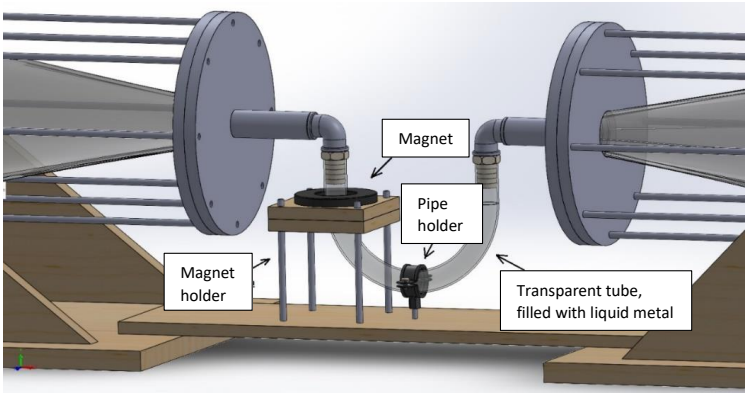

a)

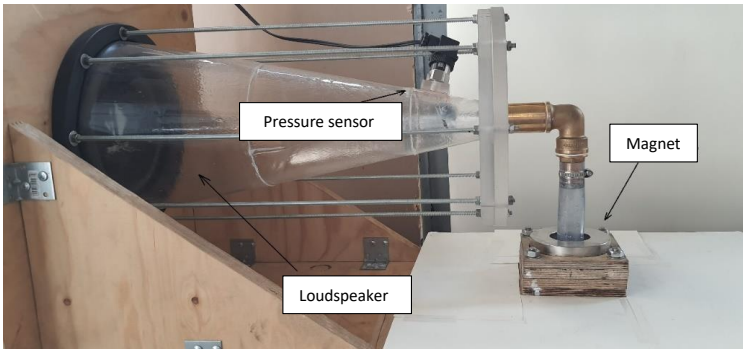

b)

Fig. 4.9. a) – Overview and zoom of the developed loudspeaker stand 3D model with explanations; b) – half of the manufactured speaker stand together with the test section.

The justification for such a hypothesis is the information found in the latest MHD literature about the possibilities of stabilizing streamwise, constant-orientation electrically conductive liquid flows with an applied magnetic field directed in the same direction as the liquid flow

[52], [53]. However, an important difference is that the flows discussed in the mentioned literature are not oscillating and, therefore, have a constant direction. For this reason, at the moment, there is actually no scientific literature on the stabilization of the corresponding studied flow. This is also understandable since there have been very few applications for alternating direction oscillating flows of electrically conductive fluids so far.

As for the instability itself, a related effect of this type has long been referred to as the Faraday instability in the hydrodynamics literature [54]. This phenomenon is observed when a volume of liquid with an open upper free surface is subjected to vertical vibrations [55]. When the acceleration of movement exceeds a particular critical value (Faraday threshold), the flat hydrostatic surface of the liquid becomes unstable and begins to ripple [56], [57]. The mechanism of occurrence and formation of these so-called Faraday waves has been relatively widely studied; for example, it is known that the frequency of the induced waves is half of the applied vibration frequency [58]. However, many related aspects are still unclear. Among them, it can be attributed to the interaction of the free surface of a liquid, electrically conductive media with a magnetic field.

In order to experimentally demonstrate the operation of the proposed stabilization method, a separate test stand was made (Fig. 4.9). It consists of two Helix Q 10W subwoofers placed opposite each other with a long-term permissible rated nominal power of 500 W. Loudspeakers, through a 1 kW D-class audio amplifier Behringer NX1000, are connected to a sinusoidal signal generator M&R Systems WG-820. Electrically, they are connected in such a way that when a sinusoidal signal is applied, their membranes move in anti-phase, i.e. in "push-pull" mode, similar to the compressor stand described in the previous sections. Also, in this case, the purpose of the experiment is to model the operation of the thermoacoustic engine. A transparent cone made of plexiglass with a transition to a smaller diameter is attached to each speaker. A 90° elbow connector continues from the cone, to which, similarly to the compressor experiment, a U-shaped transparent rubber tube filled with liquid metal – InGaSn (India-Gallium-Tin) eutectic alloy is connected. As the speaker membranes vibrate, the liquid metal can be oscillated. InGaSn is used to model sodium movement. The specific choice is based on the InGaSn eutectic's low melting point, ability to remain liquid at room temperature, lower aggressiveness, and easier manipulation of the metal. At the same time, it has been taken into account that the density of InGaSn is significantly higher than that of Na. Due to the limited power of the speakers, their ability to perform gas-liquid displacement is limited, so the amount of liquid used has been minimized as much as possible, and about 70 mL of InGaSn was used. An axially magnetized NdFeB ring type permanent magnet is placed in one level coaxially with the liquid metal free surface, as shown in Fig. 4.9, which creates a magnetic field according to the scheme in Fig. 4.8.

The experiments were carried out with a video camera filming the free surface at different angles during its movement. In Fig. 4.10 it can be seen in the visible results that the predicted expected electromagnetic stabilization effect has been observed. A reduction in the intensity of the splashes is clearly visible and a reduction in the height of the rising liquid metal splashes is observed. At the same time, it should be noted that surface waves are still observable and not completely suppressed. The following reasons are possible for this. In order to ensure

sufficiently strong magnetohydrodynamic interaction, a strong magnetic field and/or electrical conductivity of the liquid must be present. The electrical conductivity of InGaSn is several times lower than that of Na. On the other hand, the used NdFeB permanent magnet is only able to provide a relatively weak magnetic field. It was measured, and the axial field component in the center was 0.26 T, while at the inner wall of the magnet, in the middle of the magnet – 0.505 T. As can be seen, in addition to that, the distribution of the magnetic field is also inhomogeneous. Also, this could have a negative impact on the electromagnetic stabilization effect compared to a potentially homogeneous field.

At the same time, it should be noted that for the proposed stabilization method an obvious drawback can be seen in the scheme in Fig. 4.8, which is due to the limited dimensions of the magnet. The configuration of the magnetic field for an axially magnetized permanent magnet is characterized by the fact that a pronounced vertical component of the field is in the middle of the magnet, that is, in the region of the free surface of the liquid. Below this region (inside the liquid), the magnetic flux lines bend and close. Position 4 of the scheme shows the clearly visible sectors in which the fluid flow will split the magnetic field lines in any case. This will clearly cause an additional increase in hydraulic resistance due to the induced currents in these areas, which will inevitably result in hydraulic losses. Quantification of these hydraulic losses would be necessary in future studies.

Fig. 4.10. InGaSn free surface electromagnetic stabilization experiment at 20 Hz:
a) with applied magnetic field (above); b) – without magnetic field (bottom).

MAIN RESULTS AND CONCLUSIONS

In Chapter 1

1. An electric machine based on a fundamentally new concept and a unique operating principle was studied and manufactured together with its driving equipment.
2. The novelty of the manufactured and researched electric machine is based on the fact that the MHD generator is of the induction type, unlike the previously well-known MHD generators of the conduction type.
3. An induction-type MHD generator can be realised by generating an alternating flow of electrically conductive fluid in a magnetic field due to the used thermoacoustic effect.

In Chapter 2

4. A complete MHD generator calculation method is developed, which is based on the use of the equivalent circuit of the electric transformer to obtain machine parameters.
5. An automated calculation program was created in the "Visual Basic for Applications" (VBA) programming environment, which also takes into account the armature reaction, namely the effect of the secondary, demagnetizing magnetic field of the electric machine.
6. An analytical technique is proposed for the calculation of the currents induced in the liquid metal of the MHD generator based on the calculation methods of conduction-type MHD pumps found in the literature. Analytical results are compared with numerical models developed in the Quickfield environment, and a good agreement is obtained.

In Chapter3

7. A different MHD generator calculation method has been developed, which, unlike the transformer equivalent circuit described in Chapter 2, uses Maxwell's equations in the integral form, written as voltage equations.
8. It is shown that both proposed methods work equally well. The fundamental differences between the two methods are pointed out, which include the MHD generator inductance and the Na velocity, that is, how the mentioned quantities are operated in each method.
9. Using the developed methods, the possibilities of increasing the energy and power parameters of the MHD generator have been analyzed, such as the efficiency and the developed electrical power.
10. The necessity to reduce the mass of liquid metal of the electric machine as much as possible is justified. This is demonstrated by the significant role and importance of sodium inertia during the operation of the MHD generator. This justification is shown with both developed calculation methods, namely in Chapters 2 and 3 of the Thesis.

In Chapter 4

11. Independent experiments with each of the machines have been conducted. Both separately with a thermoacoustic engine and separately with an MHD generator. This was done with the aim to study the SpaceTRIPS technology in as much detail as possible.
12. The separate experiments of the TAc engine show that the machine is capable of developing a gas pressure oscillation amplitude of up to 2.7 bar at 40 bar mean pressure, which is sufficient to ensure adequate movement of liquid metal in the case if an MHD generator with liquid sodium as a working body is connected to the TAc engine.
13. As a result of the TAc experiment session, the critical excitation curve of the engine was obtained, which determines the limit of the regenerator temperature difference and mean pressure at which the engine is able to induce sound waves and work independently.
14. The electric machine testing concept is proposed, and in accordance with it, an MHD generator individual testing bench based on a two-piston compressor is developed and constructed. Using the bench, MHD generator experiments with Na were performed, and it was shown that the electric machine under study is capable of generating a sinusoidal AC voltage.
15. Before the sodium tests, an additional feasibility study experiment was performed on the compressor stand with water instead of Na. In the course of the experiment, a fundamental drawback of the MHD generator was observed and identified, namely the occurrence of instability of the free surface of the liquid metal as a result of surface movement.
16. Floats were designed and manufactured as an experimental temporary solution for free surface instability damping. Tests were carried out with both water and sodium, and a significant reduction in splashes was obtained.
17. It has been proven that the manufactured MHD generator, in combination with the TAc engine, is able to work while being coupled and develops useful electrical power at the output of the machine, which can be used by a consumer of electrical energy.
18. Analyzing the changes in gas pressure oscillations developed by the TAc engine, it was concluded from the results of the combined TAc + MHD experiment that a small effect of the operation of the MHD generator on the engine can be observed at the moment when the electric load is connected to the generator. This is explained by the counteraction of the magnetic field of the current induced in the generator coil to the movement of Na.
19. The experimentally extracted MHD generator electrical power in the TAc + MHD test was compared with the theoretically calculated one, and a good agreement of the results was obtained. The comparison was made using the theoretical model proposed in Chapter 3, which considers the ratio of the electric power developed by the MHD generator to the pressure difference supplied by the TAc engine.
20. The laboratory tests of the SpaceTRIPS prototype were performed in low power mode. However, the calculations performed in the Thesis show that the maximum potential efficiency of the device in the most favorable conditions can significantly exceed the efficiencies of competing thermoelectric converters.

21. A method for electromagnetic stabilization of the liquid metal free surface with the use of a permanent magnetic field was developed and presented.
22. A modeling bench was developed for testing the proposed stabilization method, which is based on two oppositely placed and anti-phase “push-pull” mode vibrating loudspeakers.
23. A modeling experiment for visualization of the developed method was carried out with InGaSn eutectic alloy. It has been proven and shown that with the help of an electromagnetic field, according to the scheme developed by the author, it is possible to reduce the liquid metal splashes generated during the operation of the MHD generator and, to a certain extent, stabilize the free surface of liquid metal.

REFERENCES

[1] "What Powers a Spacecraft?" 2019. https://spaceplace.nasa.gov/what-powers-a-spacecraft/en/.

[2] "Basics of Space Flight – Inverse square law." https://solarsystem.nasa.gov/basics/chapter6-1/.

[3] N. T. Redd, "NASA's Juno Mission to Jupiter to Be Farthest Solar-Powered Trip," 2011. https://www.space.com/12541-juno-jupiter-mission-solar-panels-power.html.

[4] F. Morring, "Space Nuclear Power," *Aviat. Week Sp. Technol. (New York)*, vol. 160, no. 22, pp. 537–553, Jan. 2003, doi: 10.1016/B0-12-227410-5/00715-8.

[5] G. L. Bennett, "Introduction to Space Nuclear Power and Propulsion," *Encycl. Nucl. Energy*, pp. 155–167, Jan. 2021, doi: 10.1016/B978-0-12-819725-7.00133-1.

[6] J. Sharp, "Thermoelectric Energy Conversion Devices," *Ref. Modul. Mater. Sci. Mater. Eng.*, Jan. 2016, doi: 10.1016/B978-0-12-803581-8.01093-6.

[7] G. Benvenuto and F. de Monte, "Analysis of free-piston Stirling engine linear alternator systems," *J. Propuls. power*, vol. 11, no. 5, 1995.

[8] D. Zudell, "Stirling Convertor Sets 14-Year Continuous Operation Milestone," 2020. https://www.nasa.gov/feature/glenn/2020/stirling-convertor-sets-14-year-continuous-operation-milestone.

[9] C.-H. Cheng and H.-S. Yang, "Stirling Engine Technology and Its Application on Solar Power Generation," in *Innovative Design, Analysis and Development Practices in Aerospace and Automotive Engineering*, 2014, pp. 3–9.

[10] S. Backhaus and G. W. Swift, "2. A thermoacoustic-Stirling heat engine: Detailed study.pdf," *J. Acoust. Soc. Am.*, vol. 107, no. 6, pp. 3148–3166, 2000.

[11] S. Backhaus and G. Swift, "New Varieties of Thermoacoustic Engines," *Ninth Int. Congr. Sound Vib.*, pp. 1–8, 2002, [Online]. Available: http://www.lanl.gov/thermoacoustics/Pubs/ICSV9.pdf.

[12] M. Veselý and T. Vít, "Difference between working gases in thermoacoustic engine," 2014, doi: 10.1051/C.

[13] K. Wang *et al.*, "Experimental Study on a 500 W Traveling-wave Thermoacoustic Electric Generator," *Energy Procedia*, 2014.

[14] H. Kang, P. Cheng, Z. Yu, and H. Zheng, "A two-stage traveling-wave thermoacoustic electric generator with loudspeakers as alternators," *Appl. Energy*, vol. 137, pp. 9–17, 2015, doi: 10.1016/j.apenergy.2014.09.090.

[15] A. Al-Kayiem and Z. Yu, "Design of a Traveling Wave Thermoacoustic Engine Driven Cooler with Hybrid Configuration," *World Congr. Eng.*, vol. II, pp. 1–6, 2014, doi: 2078-0958.

[16] E. A. Zinoviev, G. V. Vorotnikov, A. I. Dovgyallo, and S. O. Nekrasova, "Boundaries of thermoacoustic instability in the thermoacoustic engine with cryogenic cooling," *J. Int. Acad. Refrig.*, vol. 19, no. 4, 2020, doi: 10.17586/1606-4313-2020-19-4-20-26.

[17] I. Girgin and M. Türker, "THERMOACOUSTIC SYSTEMS AS AN ALTERNATIVE TO CONVENTIONAL COOLERS," *MSU Barbar. Nav. Sci. Eng. Inst.*, vol. 8, pp. 14–32, Apr. 2011.

[18] D. McKelvey, S. Ballaster, and S. Garrett, "Shipboard electronics thermoacoustic cooler," Naval Postgraduate School Monterey, California, 1995.

[19] S. L. Garrett, J. A. Adeff, and T. J. Hofler, "Thermoacoustic refrigerator for space applications," *J. Thermophys. Heat Transf.*, vol. 7, no. 4, pp. 595–599, 1993, doi: 10.2514/3.466.

[20] V. S. Slavin, G. C. Bakos, T. A. Milovidova, and K. A. Finnikov, "Space power

installation based on solar radiation collector and MHD generator," *IEEE Trans. Energy Convers.*, 2006, doi: 10.1109/TEC.2005.860401.
[21] D. W. Price *et al.*, "Pamir-3U Magnetohydrodynamic generator results," 1995.
[22] D. W. Swallom *et al.*, "Results from the Pamir-3U pulsed portable MHD power system program," 1996.
[23] Y. Wang, X. Duan, P. Yan, H. Xue, and Q. Li, "A pulsed magnetohydrodynamic generator for electric launcher," 2005, doi: 10.1109/TMAG.2004.838972.
[24] L. Hu, H. Kobayashi, and Y. Okuno, "Performance of a Liquid Metal MHD Power Generation System for Various External Forces," Jul. 2014, doi: 10.2514/6.2014-3558.
[25] A. Geri, G. M. Veca, and A. Salvini, "Performance evaluation of MHD generators: Applications," *IEEE Int. Electr. Mach. Drives Conf. Rec. IEMDC*, pp. 10–12, 1997, doi: 10.1109/iemdc.1997.604139.
[26] Jyoti Gupta, Manish Kumar Singla, and Parag Nijhawan, "Magnetohydrodynamic system – a need for a sustainable power generation source," *Magnetohydrodynamics*, vol. 57, no. 2, pp. 251–272, 2021, doi: 10.22364/mhd.57.2.9.
[27] N. Rott, "Thermoacoustics," in *Advances in Applied Mechanics*, Vol. 20., C.-S. Yih, Ed. Michigan: Elsevier, 1980, pp. 135–174.
[28] Ю. Бирзвалк, *Основы теории и расчёта кондукционных МГД-насосов постоянного тока*. Рига: Зинатне, 1968.
[29] И. М. Толмач and Е. И. Янтовский, *Магнитогидродинамические генераторы*. Москва: Наука, 1972.
[30] Ситтиг, *Натрий, его производство, свойства и применение*. Москва: Госатомиздат, 1961.
[31] C. H. Hansen, "Fundamentals of acoustics," 1951.
[32] A. T. A. M. De Waele, "Basic operation of cryocoolers and related thermal machines," *J. Low Temp. Phys.*, vol. 164, no. 5–6, pp. 179–236, 2011, doi: 10.1007/s10909-011-0373-x.
[33] Gregory W. Swift, *Thermoacoustics A Unifying Perspective for Some Engines and Refrigerators, Second Edition*. 2018.
[34] M.-X. Francois *et al.*, "The SpaceTRIPS project: Space thermoacoustic radioisotopic power system," in *Proceedings of 23rd Conference of the Italian Association of Aeronautics and Astronautics AIDAA2015*, 2015, pp. 17–19.
[35] A. Brēķis, J. E. Freibergs, and A. Alemany, "Space thermo acoustic radio-isotopic power system: Space trips," *Magnetohydrodynamics*, vol. 55, no. 1–2, pp. 5–14, 2019, doi: 10.22364/mhd.55.1-2.1.
[36] G. Benvenuto and G. Bisio, "Thermoacoustic systems, Stirling engines and pulse-tube refrigerators: analogies and differences in the light of generalized thermodynamics," in *Proceedings of the 24th Intersociety Energy Conversion Engineering Conference*, 1989, pp. 2413–2418 vol.5, doi: 10.1109/IECEC.1989.74812.
[37] A. Brēķis, "Termoakustiskā maiņstrāvas magnetohidrodinamiskā ģeneratora teorētiskā un eksperimentālā izpēte, Maģistra darbs," RTU, 2017.
[38] О. А. Лиелаусис, *Гидродинамика жидкометаллических МГД-устройств*. Рига: Зинатне, 1967.
[39] А. В. Тананаев, *Гидравлика МГД машин*. Москва: Атомиздат, 1970.
[40] Я. Я. Лиелпетер, *Жидкометаллические индукционные МГД-машины*. Рига: Зинатне, 1969.
[41] А. И. Вольдек, *Индукционные магнитогидродинамические машины с жидкометаллическим рабочим телом*. 1970.
[42] A. Gailītis and A. Brēķis, "Equivalent circuit approach for acoustic mhd generator," *Magnetohydrodynamics*, vol. 56, no. 1, pp. 3–13, 2020, doi: 10.22364/mhd.56.1.1.

[43] T. A. Ltd., “Quickfield ‘Active Field’ tehnoloģijas apraksts.” https://active.quickfield.com/HTML/Welcome.htm.
[44] L. Lavrinoviča, “Promocijas darbs: Bezkontaktu sinhrono dzinēju izstrāde un optimizācija izmantošanai mazjaudas elektroiekārtās,” 2014.
[45] A. Brekis, A. Alemany, O. Alemany, and A. Montisci, “Space Thermoacoustic Radioisotopic Power System, SpaceTRIPS: The Magnetohydrodynamic Generator,” *Sustainability*, vol. 13, no. 23, 2021, doi: 10.3390/su132313498.
[46] A. Brēķis, A. Alemany, and J. Freibergs, “Analysis of magnetohydrodynamic generator driven by thermoacoustic engine for deep Space applications,” Nov. 2020, doi: 10.1109/RTUCON51174.2020.9316584.
[47] И. М. Кирко, *Жидкий металл в электромагнитном поле (электронная книга)*. Москва, Ленинград: Энергия, 1964.
[48] И. М. Кирко *et al.*, *Прикладная магнитная гидродинамика - учебное пособие по теоретическому курсу*. Красноярск: Сибирский федеральный университет, 2007.
[49] Л. А. Верте, *Магнитная гидродинамика в металлургии*. Москва: “Металлургия,” 1975.
[50] A. Alemany, A. Krauze, and M. Al Radi, “Thermo acoustic – MHD electrical generator,” *Energy Procedia*, vol. 6, pp. 92–100, 2011, doi: 10.1016/j.egypro.2011.05.011.
[51] M. A. G. Timmer, K. de Blok, and T. H. van der Meer, “Review on the conversion of thermoacoustic power into electricity,” *J. Acoust. Soc. Am.*, vol. 143, no. 2, pp. 841–857, Feb. 2018, doi: 10.1121/1.5023395.
[52] Y. Kolesnikov, D. Krasnov, and T. Boeck, “Evolution of a round jet in a duct in the presence of a uniform axial magnetic field,” *Magnetohydrodynamics*, vol. 53, no. 1, pp. 119–127, 2017, doi: 10.22364/mhd.53.1.13.
[53] P. Vieweg, Y. Kolesnikov, and C. Karcher, “EXPERIMENTAL STUDY OF A LIQUID METAL FILM FLOW IN A STREAMWISE MAGNETIC FIELD,” in *Proceedings of the 10th international conference “Electromagnetic Processing of Materials 2021,”* 2021, pp. 150–154.
[54] M. Faraday, “On a Peculiar Class of Acoustical Figures; and on Certain Forms Assumed by Groups of Particles upon Vibrating Elastic Surfaces,” *Philos. Trans. R. Soc. London*, vol. 121, pp. 299–340, Jan. 1831, [Online]. Available: http://www.jstor.org/stable/107936.
[55] X. Zhao, J. Tang, and J. Liu, “Electrically switchable surface waves and bouncing droplets excited on a liquid metal bath,” *Phys. Rev. Fluids*, vol. 3, no. 12, pp. 1–14, 2018, doi: 10.1103/PhysRevFluids.3.124804.
[56] Л. Ландау and Е. Лифшиц, *Теоретическая физика, Том I, Механика*. Москва: Наука, 1988.
[57] Е. М. Лифшиц and Л. П. Питаевский, *Теоретическая физика, Том X, Физическая Кинетика*. Москва: Наука, 1979.
[58] H. W. Müller, H. Wittmer, C. Wagner, J. Albers, and K. Knorr, “Analytic stability theory for faraday waves and the observation of the harmonic surface response,” *Phys. Rev. Lett.*, vol. 78, no. 12, pp. 2357–2360, 1997, doi: 10.1103/PhysRevLett.78.2357.

Artūrs Brēķis was born in 1992 in Riga. He obtained a Bachelor's degree in Electrical Power Engineering (2014), qualification of an electrical engineer with distinction (2016), as well as a professional Master's degree in Computerized Control of Electrical Technologies (2017) from Riga Technical University. He was multiple "Latvenergo" and "Latvian Association of Power Engineers and Energy Constructors (LEEA)" student research paper competition laureate. In 2017 he was included in the "Golden Fund" of RTU graduates. From 2015 to 2017 he was a research assistant with the Institute of Physics of the University of Latvia (IPUL). Since 2017, he has been a researcher with the IPUL Laboratory of Magnetic Hydromechanics. In 2016, he had an internship at the Sardinian Energy Research Laboratory "Sardegna Ricerche", Italy. In parallel with his scientific work at the IPUL, since 2021, he has been teaching the fundamentals of electrodynamics at the RTU Department of Electrical Machines and Apparatus. His scientific interests are related to space technologies, magnetohydrodynamics, liquid metals and thermoacoustics.